









Photonic van der Waals integration from 2D materials to 3D nanomembranes

Yuan Meng ^{1,10}, Jiangan Feng ^{2,10}, Sangmoon Han^{1,10}, Zhihao Xu ³, Wenbo Mao ⁴, Tan Zhang², Justin S. Kim³, Ilpyo Roh¹, Yepin Zhao⁵, Dong-Hwan Kim^{6,7}, Yang Yang ⁵, Jin-Wook Lee ^{8,9} ✉, Lan Yang^{3,4} ✉, Cheng-Wei Qiu ² ✉ & Sang-Hoon Bae ^{1,3} ✉

Abstract

The integration of functional nanomaterials and heterostructures with photonic architectures has laid the foundation for important photonic and optoelectronic applications. The advent of epitaxy and layer lift-off techniques has enabled a wide spectrum of two-dimensional materials and three-dimensional single-crystalline freestanding thin films with diverse optical functionalities, featuring van der Waals (vdW) interfaces suitable for photonic vdW integration. Physical assembly leveraging vdW interactions eliminates the constraints of epitaxial lattice-matching, introducing unprecedented freedom to combine dissimilar materials with appealing optoelectronic properties but radically distinct crystal structures. Various prefabricated vdW building blocks can be combined in novel hetero-integrated photonic architectures and hybrid vdW heterostructures to prototype new devices and explore exotic nanophotonic phenomena at mixed-dimensional vdW interfaces. The ultrathin nature of these freestanding nanomembranes also enables flexible and lightweight photonic devices for low-cost wearable and multifunctional health-care applications. In this Review, we survey the recent progress in photonic nanomembranes with vdW interfaces, discussing a broad range of delaminated freestanding nanomembranes from film preparation to device implementation. We also analyse the remaining challenges and highlight emerging opportunities for advanced vdW hetero-integration.

Sections

Introduction

Freestanding films for photonic vdW integration

Applications of 2D photonic vdW films

Applications of 3D photonic freestanding films

Photonic applications of vdW heterostructures

Outlook

A full list of affiliations appears at the end of the paper. ✉ e-mail: jw.lee@skku.edu; lyang25@wustl.edu; chengwei.qiu@nus.edu.sg; sbae22@wustl.edu

Introduction

The integration of functional materials with photonic structures not only underpins a broad spectrum of optical and optoelectronic applications, but also enables the exploration of novel nanophotonic phenomena in heterostructures^{1,2}. Integrated photonics based on silicon (Si) and silicon nitride (SiN) enables a vast range of technologies³, from information processing and communications⁴ to imaging⁵, bio-sensing⁶ and displays. Nevertheless, single-material platforms have various intrinsic shortcomings. The long-term vision is to integrate different optical materials into a single photonic chip to realize devices covering functionalities from light generation to modulation, propagation and detection⁷. Novel platforms for the heterogeneous integration of dissimilar functional materials thus attract strong interest from both academy and industry⁸.

Conventional integration strategies relying on heteroepitaxy are limited by the difficulty of combining materials with different crystal structures owing to the stringent requirements for lattice matching and processing compatibility. In the epitaxial growth of three-dimensional (3D) crystals, strong chemical bonds are formed between the epilayer and substrate. To obtain single-crystalline epilayers, the grown material generally needs to have the same crystal structure as the substrate, and their lattice parameters should not differ by more than a few per cent⁹ or else defects tend to be generated beyond a certain critical film thickness via strain relaxation mechanisms¹⁰. When there is a significant lattice discrepancy with the substrate, polycrystalline phases emerge. Sometimes only epitaxial islands are formed, preventing uniform thin-film growth and good material performance¹¹. These restrictions greatly limit the possible material combinations for hetero-integration, hindering potential applications¹². Non-epitaxial approaches such as physical vapour deposition have no lattice-matching constraints, but the deposited materials are typically defective and are amorphous or polycrystalline, with substantially worse intrinsic properties compared with their single-crystalline counterparts¹¹.

Van der Waals (vdW) integration, a concept originally proposed for two-dimensional (2D) materials^{11,13}, offers an alternative way of integrating highly disparate materials with unprecedented flexibility. High-quality building blocks with desired optical attributes can be pre-fabricated and assembled through vdW interactions, regardless of their lattice parameters, crystal structures or orientation^{14,15}. Because it does not involve one-to-one chemical bonds between adjacent layers, this approach enables the fabrication of mixed-dimensional vdW heterostructures and novel moiré superlattices via layer transfer, eliminating the lattice compatibility requirement of epitaxy. This approach was successfully applied in 2D photonics, including in integrated photonics and in the study of polariton physics^{16–19}.

Research on 2D materials has attracted tremendous attention in the past decade, but recent years have also witnessed exciting progress in 3D crystalline nanomembranes with diverse functionalities that can be exfoliated into freestanding forms^{8,20}. Advanced epitaxy and layer lift-off technologies^{21–24} can provide single-crystalline 3D freestanding films with atomically clean and electronically sharp vdW interfaces for numerous photonic and optoelectronic applications. Unlike 2D materials, which are intrinsically layered atomic lattices with intralayer covalent bonds and interlayer vdW interactions¹³, in 3D ‘artificial vdW films’ there are chemical bonds between the layers inside the film (Fig. 1a, top)^{25–27}. However, like 2D materials, 3D nanomembranes are typically thin and have clearly terminated boundaries featuring vdW interfacial interactions²⁰.

These properties raise the possibility that 3D crystals, like 2D materials, can also be made ultrathin, flexible, stackable into heterostructures

with substantial interlayer lattice discrepancies via vdW forces, and transferable to arbitrary photonic templates. Furthermore, whereas 2D materials usually exhibit exotic properties only at a thickness of a few monolayers¹⁴, 3D freestanding films exhibit optical attributes similar to those of their bulk counterparts almost independently of thickness^{8,20}. 3D nanomembranes thus have potential for applications that require substantial interaction thickness, as exemplified by recent successes obtained with hybrid III–V-on-Si platforms^{28,29} and thin-film lithium niobate photonics^{30,31}.

In this Review, we discuss recent advances in photonic vdW integration based on functional freestanding nanomembranes with vdW interfaces. We present a comprehensive survey of 2D and 3D freestanding films, from film preparation to device implementation. The fundamental photonic properties of these vdW films and their hybrid heterostructures are catalogued with representative applications: 2D and 3D freestanding films constitute a wide library of vdW building blocks with diverse functionalities, and can act as the optical gain, photovoltaic, electro-optical (EO) or magneto-optical (MO) medium, creating new opportunities in photonic hetero-integration. These heterostructures also provide an ideal playground in which to investigate exotic polaritonic phenomena, for example in nanophotonic moiré superlattices formed at mixed-dimensional vdW interfaces^{1,20}. Novel optical applications can be prototyped by leveraging the physical couplings between 2D/3D freestanding nanomembranes and photonic structures^{15,32,33}. We also discuss practical challenges and emerging opportunities for advanced photonic hetero-integration, including vdW meta-photonics, and flexible and bio-compatible optical applications.

Freestanding films for photonic vdW integration

High-quality 2D and 3D functional optical layers with vdW interfaces can be prepared on different substrates and subsequently transferred to arbitrary photonic templates like Lego bricks (Fig. 1a). This opens up unique advantages²⁰.

- **Advanced hetero-integrated photonics.** Given that no covalent bond generally exists between the freestanding nanomembranes and host substrate, the 2D and 3D freestanding films can be delaminated and transferred to couple with arbitrary off-the-rack optical structures^{12,13}. Record-setting devices and multifunctional optical systems can be envisaged in previously inaccessible hetero-integration layouts^{7,8,11,34}, without the need for the expensive facilities and lengthy development processes required by epitaxial approaches.
- **Novel heterostructure physics.** Single-crystalline 3D nanomembranes can be selectively stacked and mixed with 2D monolayers to obtain heterostructures with exotic hybrid interfacial phenomena involving vdW photons, excitons and phonons^{1,15}.
- **Vertical integration.** Conventional integrated photonics deploys devices along the plane of a wafer³. The advent of high-quality 2D and 3D freestanding films enables novel device and circuitry architectures along the vertical direction, which has previously been not well explored. By stacking the functional vdW building blocks perpendicularly via layered fabrication processes, 3D integration enables multifunctional photonic systems with dense vertical connectivity, speed and energy efficiency between neighbouring layers^{35,36}.
- **Flexible and bio-compatible optical applications.** 2D materials show intrinsically high mechanical flexibility, which is advantageous for stretchable applications²⁹. The ultrathin nature of isolated 3D crystalline membranes is also compatible with wearable

optical devices (which are bendable, albeit less stretchable than those based on 2D films, unless special treatments are applied³⁷) and nanophotonic biosensors³⁸.

• Cost reduction. Despite the advantageous optoelectronic properties of group III–V and nitride semiconductors, which enable record-breaking devices^{7,28,29}, they are less widespread in

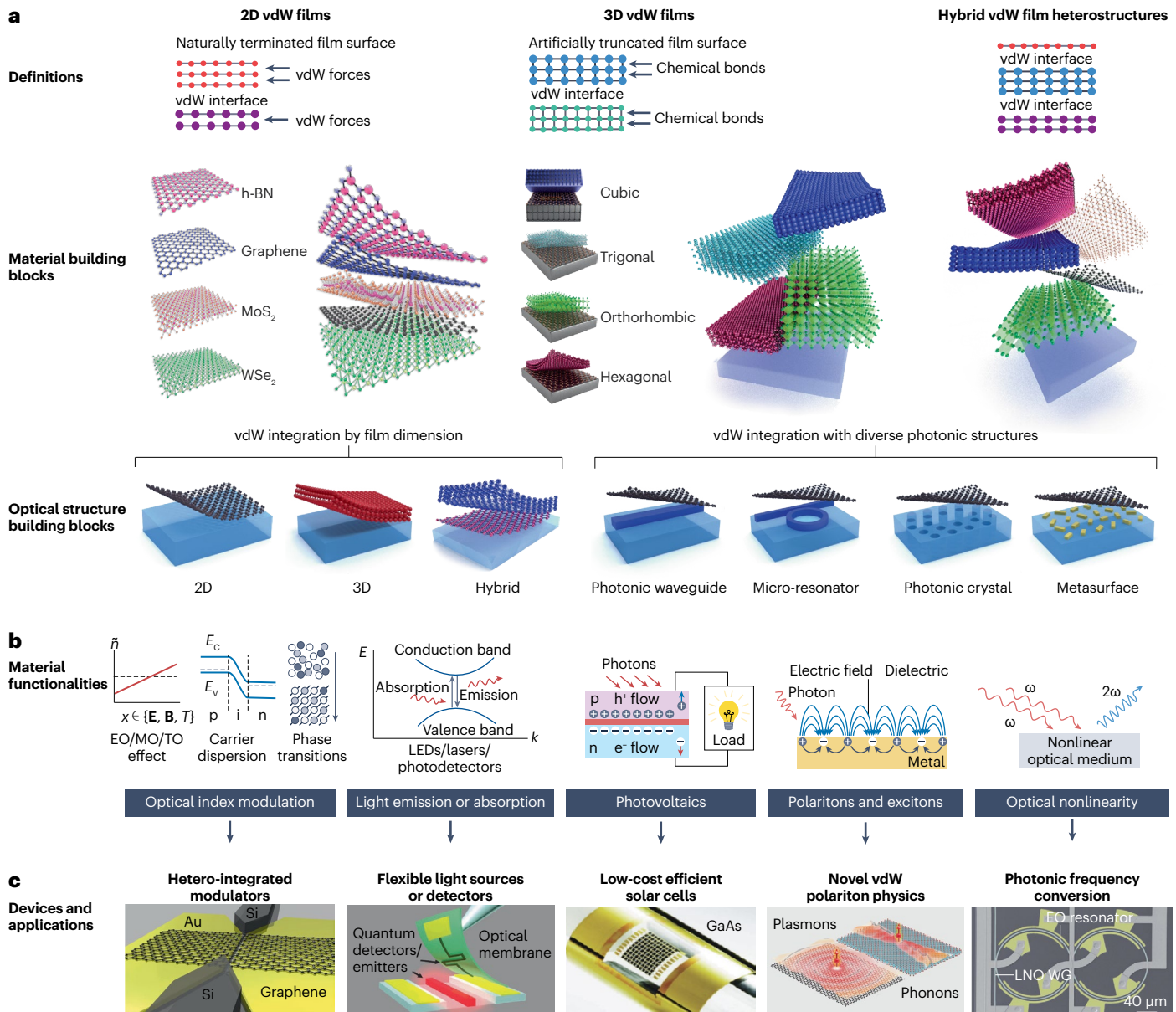


Fig. 1 | Freestanding functional nanomembranes for photonic vdW integration. **a**, Two-dimensional (2D) van der Waals (vdW) films are monolayer lattices with intralayer covalent bonds and interlayer vdW interactions^{9,12}. By contrast, three-dimensional (3D) freestanding films feature intralayer chemical bonds as in the bulk and clearly truncated boundaries artificially created via layer lift-off techniques²². Both 2D and 3D nanomembranes possess vdW interfaces and various optoelectronic functionalities, and can be used as building blocks for photonic vdW integration. **b**, Exemplary material functionalities, including modulation of the optical index \tilde{n} via electro-optical (EO), magneto-optical (MO), thermal-optical (TO) effects, carrier dispersion or phase transitions; light emission or absorption in direct bandgap materials; photovoltaic properties; generation of surface polaritons; and optical nonlinearity. **c**, Applications corresponding to the functionalities in panel **b**, including a graphene-laminated

gold plasmonic modulator¹⁵³, a single-photon detector³⁴, a flexible GaAs nanomembrane photovoltaic cell²¹², a device supporting vdW plasmon-polaritons and phonon-polaritons¹, and a wafer-bonded thin-film LiNbO₃ waveguide (LNO WG) frequency shifter based on an EO resonator⁶⁹. ω , light frequency; \mathbf{E} and \mathbf{B} are the electric and magnetic fields; E_c and E_v are the conduction and valence band edges; h^+ and e^- , hole and electron; h-BN, hexagonal boron nitride; i, intrinsic; LED, light-emitting diode; p and n, positive and negative doping; T is temperature. Panel **c** (hetero-integrated modulators) adapted from ref. 153, Springer Nature Limited. Panel **c** (flexible light sources or detectors) adapted from ref. 34, CC BY 4.0. Panel **c** (low-cost efficient solar cells) adapted from ref. 212, Springer Nature Limited. Panel **c** (novel vdW polariton physics) adapted from ref. 1, Springer Nature Limited. Panel **c** (photonic frequency conversion) adapted from ref. 69, Springer Nature Limited.

the market than Si photonic devices. An important reason is the high cost of their wafers compared with Si (ref. 39). For most applications, the functional part is the top thin device layer, and the costly substrate serves only as a mechanical support. Advanced epitaxy^{23,40} and layer lift-off technologies enable wafer recycling and mass manufacture of functional freestanding nanomembranes^{23,41,42}, which is promising for the cost reduction and commercialization of non-Si optical materials^{8,43}.

Next, we outline the fundamental photonic and optoelectronic properties of freestanding nanomembranes for vdW integration and discuss their primary coupling mechanisms with different photonic structures.

Features of photonic vdW films

vdW films can be categorized into conventional 2D nanosheets and isolated 3D freestanding nanomembranes²³ with vdW interfaces for constructing mixed-dimensional vdW heterostructures. They can also be grouped by their optical functionalities (gain, photovoltaic, TO, EO, MO and piezoelectric materials⁴⁴, Fig. 1b), electronic behaviours (metals, semiconductors and insulators), or crystal parameters (crystallinity, lattice structure and orientations)^{9,11}.

2D vdW films. 2D vdW films are typically one to a few layers thick and display fascinating properties^{45,46} (Table 1). These attributes, along with their atomically clean vdW interfaces, are well suited to building artificial vdW heterostructures^{11,12}, making these materials a prominent research direction in photonics, material science and nanotechnology⁴⁵.

However, the very small thickness of 2D materials greatly restricts the spatial light–matter interaction length⁴⁷, and their bandgaps generally depend strongly on the number of atomic layers. For instance, in transition metal dichalcogenides (TMDs) the bandgap transits from indirect to direct when moving from bulk to monolayer samples¹⁷.

3D freestanding films. Unlike 2D materials, which are made of intrinsic atomic monolayers that can be mechanically exfoliated along layered vdW interfaces, 3D nanomembranes are made into freestanding forms with artificially terminated vdW interfaces using specific epitaxial and layer delamination techniques^{21–23,28}. Moreover, the chemical and optical properties of freestanding 3D films are similar to those of the bulk materials²⁰ (Table 1). Changing the thickness of 3D freestanding films typically affects only their mechanical properties, such as Young’s modulus and stiffness, but not the bandgap²³, which is advantageous for wearable optics (which cannot be realized with rigid bulk materials⁴⁸) and for applications such as optical amplifiers, modulators and nonlinear photonic devices that require thick media to enhance the light–matter interaction strength⁴⁹.

In addition, whereas 2D materials have challenges in doping, for 3D nanomembranes it is possible to adjust the growth parameters and chemical compositions to tailor the doping level and bandgap-determined operation wavelength²⁵. Because the 3D freestanding films are artificially delaminated, they do not require intrinsically layered vdW lattices, opening up a wide choice of available materials. Leveraging universal methods like smart-cut^{50,51}, mechanical spalling^{52–54} and 2D-assisted layer-transfer^{20,22,23}, the library of 3D freestanding films might be further extended to arbitrary bulk 3D materials. Because 3D freestanding films are artificially lifted-off from bulk crystals, dangling bonds normally still exist at the film surface¹¹.

Table 1 | Comparison of the properties of 2D and 3D freestanding thin films

Properties	2D vdW films	3D freestanding films
Material	Naturally layered structures with intralayer covalent bonds and interlayer vdW interactions	Traditional materials (no specific requirements) with chemical bonding throughout the film
Thickness	From monolayer to bulk	From typically tens of nanometres to bulk
Strengths	Exotic photonic and optoelectronic properties, such as ultrahigh carrier mobility in graphene and excitonic responses in transition metal dichalcogenides Platforms with which to study low-dimensional condensed matter physics	Broad choice of available materials with well-studied photonic functionalities Broad choice of film thicknesses that preserve the bulk properties and offer large light–matter interaction lengths
Weaknesses	Monolayer properties typically not preserved when increasing the layer number Limited light–matter interaction length Challenging to obtain large-scale high-quality 2D materials Limited library of material candidates compared with 3D nanomembranes	Specific layer delamination techniques required Lower film flexibility than 2D vdW films Dangling bonds exist at the vdW interface

vdW, van der Waals.

Functionalities of photonic vdW films

2D and 3D freestanding films have a vast range of electronic bandgaps and potential applications (Fig. 1c and Fig. 2). 2D vdW films consist of graphene, TMDs, hexagonal boron nitride (h-BN), black phosphorus (BP)^{12,45,46,55} and metal oxides and halides; these materials display exotic properties useful for optical modulation^{49,56}, nonlinear optics^{57,58}, hyperbolic polaritons^{59–61}, ferromagnetism^{62,63} and ferroelectricity⁶⁴. 3D freestanding films encompass various freestanding nanomembranes exfoliated from a variety of metals, crystalline semiconductors^{25,65} and complex oxides^{8,66}.

As the bandgap becomes wider, the electronic responses change from metallic, offering high conductivity for electrical contacts and surface plasmon polaritonic applications^{67,68}, to semiconducting (such as TMDs, BP and group IV, III–V, II–VI and IV–VI compounds)²³, and finally to insulating (for example, in wide-bandgap materials such as 2D h-BN and 3D oxides such as EO crystals of lithium niobate (LNO)^{30,69–78}, barium titanate^{79–83} and MO crystals of doped garnets^{84–86}).

2D vdW films. Benefiting from a low density of states, high carrier mobility and tuneable optical transitions⁸⁷, graphene sustains propagating plasmons and surface plasmon polaritons with low damping and broadband tuneability^{88–90}, allowing for diverse optical functionalities such as optical phase and amplitude modulation, wideband photodetection, widely tuneable surface plasmon polaritons and nonlinear optics⁹¹.

Monolayer TMDs (with formula MX₂, where M is the transition metal and X is the chalcogenide atom)⁴⁶ have a direct bandgap with tightly bound excitons (spatially separated electrons and holes that interact strongly via Coulomb forces) that result in strong light emission^{92,93}.

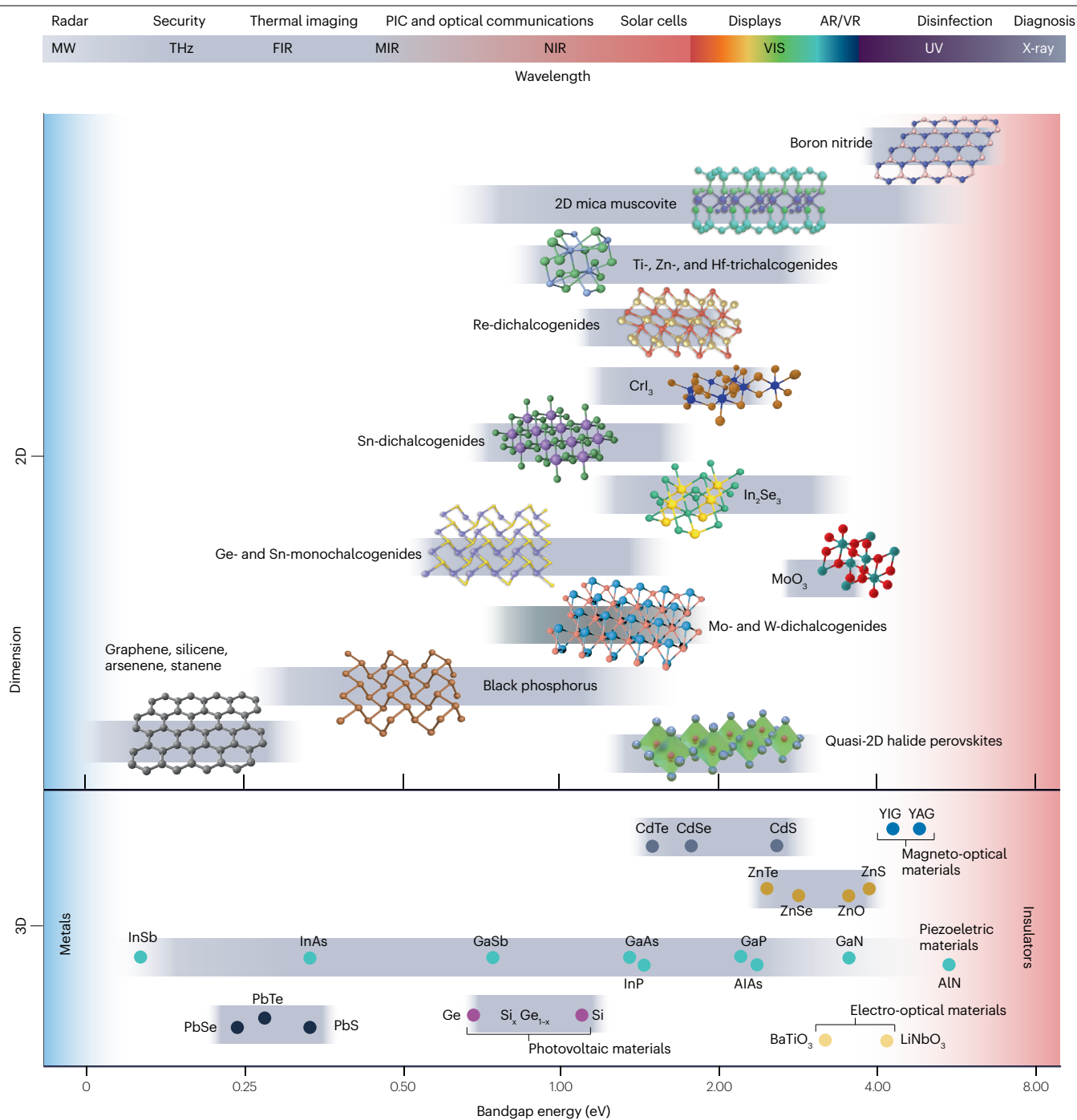


Fig. 2 | Fundamental properties of photonic vdW films. 2D and 3D freestanding films organized according to their bandgap and electronic responses. Exemplary applications are outlined according to the materials' operation wavelengths. AlN and GaN are representative piezoelectric materials; other materials in the same row, such as GaP and GaAs, also display piezoelectricity, but more weakly.

Data are from refs. [25,27,96,167](#). AR/VR, augmented reality/virtual reality; FIR, MIR and NIR, far-, mid- and near-infrared, respectively; MW, microwave; PIC, photonic integrated circuit; THz, terahertz; UV, ultraviolet; vdW, van der Waals; VIS, visible; YAG, yttrium aluminium garnet; YIG, yttrium iron garnet.

Owing to broken inversion symmetry and strong spin-orbit coupling, spin-valley locking makes TMDs an ideal platform for valleytronics, where the spin and valley degrees of freedom can be directly addressed with circularly polarized light^{94,95} (Supplementary Fig. 1a).

BP exhibits a bandgap widely tuneable from 0.3 eV (bulk) to 2.0 eV (monolayer), thus bridging the energy gap between TMDs and graphene⁹⁶. Its low-symmetry crystal lattice (D_{2h}), high carrier mobility and strong exciton resonance are useful for photonic applications such

as polarization-sensitive photodetection⁹⁷ and on-chip infrared light sources⁹⁸. vdW heterostructures comprising h-BN can exhibit intriguing photonic effects such as second-order nonlinearity⁹⁹, hyperbolic phonon polaritons¹⁰⁰ and single-photon emission¹⁰¹.

2D metal-halide perovskites, fabricated by layer-by-layer assembly of few-layer perovskites and bulky organic cations, are solution-processable 2D materials^{102–104}. These organic–inorganic hybrid quasi-2D materials display strong exciton resonances¹⁰⁵, wavelength-configurable efficient light emission^{106–108} (Supplementary Fig. 1b) and photoconductivity¹⁰⁹. The bulky interlayer cations, with their chemical diversity, can introduce emergent properties such as chirality¹¹⁰, optical nonlinearity¹¹¹ and ferroelectricity¹¹².

3D freestanding films. Owing to their abundant free electrons, noble metals are representative platforms for surface plasmon polaritons, which are collective electron oscillations under an external electromagnetic wave stimulus⁶⁷. In addition, a vast collection of metals with different work functions⁷⁰ (Supplementary Fig. 1c) enable vdW electrical contacts in optoelectronic circuits with decreased contact resistance and hysteresis^{113–115}.

Freestanding semiconductor nanomembranes display excellent photonic and optoelectronic properties at high film crystallinity²³. Advanced epitaxy allows us to tune the bandgap of these semiconductors (and their alloys) to cover a wide range of applications from terahertz to ultraviolet frequencies²⁵ (Fig. 2, top). 3D freestanding films showcase a much broader variety of chemical compositions and optical functionalities than do 2D materials^{21,22}. For instance, Si is widely used in integrated photonics³⁹ and mainstream photovoltaic materials^{39,116–118}, and group III–V materials with engineerable direct bandgaps²⁵, such as GaAs and InP, are prominent optoelectronic platforms for high-performance lasers, optical amplifiers, light-emitting diodes (LEDs) and photodetectors^{119–121}.

Insulating 3D freestanding films include many reconfigurable optical materials (Fig. 2). Their refractive index n can be modified by external physical quantities such as the electric field \mathbf{E} (EO effect), magnetic field \mathbf{B} (MO effect), strain \mathbf{F} , or temperature T (TO effect)^{119–121}. LNO is the canonical example of an EO crystal^{75–77}; its induced birefringence changes linearly with the applied electric field (Pockels effect), making this material a well-established platform for optical modulators and second-harmonic generation⁷⁰. Recently, this textbook crystal has also been used in many integrated photonic applications^{71–73,78}, thanks to the availability of high-quality LNO-on-insulator wafers made via layer bonding⁷⁰. The successful reduction of optical losses for waveguiding (Supplementary Fig. 1d) and reliable photonic integration contributed to this recent success. Other 3D freestanding films are also being developed for optical applications²⁰.

vdW heterostructures. Freestanding nanomembranes can also be combined into artificial vdW heterostructures to realize novel optical phenomena that arise from the interplay between the vertically stacked or laterally stitched vdW films^{9,14}. Heterostructures with type-II band alignment can be constructed with TMDs for ultrafast charge transfer and generation of interlayer excitons with electrons and holes confined in different layers^{122,123}, which exhibit a longer lifetime and a lower valley depolarization rate than intralayer excitons^{124,125}. Electric dipoles aligned along the out-of-plane direction underpin the electrical tuning of the resonance energy and dynamics of interlayer excitons^{126,127}. The twist angle is another important degree of freedom, enabling the formation of moiré superlattices with flat bands^{128,129} for exploring strongly

correlated systems, such as superconductors¹³⁰, Mott insulators¹³¹ and Wigner crystals¹³².

Preparation of vdW films

Two strategies exist to prepare 2D vdW monolayers^{12,20,133–135} (Fig. 3a): top-down exfoliation methods (mechanical and liquid-phase exfoliation) and bottom-up growth methods (mainly chemical vapour deposition (CVD) and related approaches). Mechanical exfoliation produces high-quality 2D flakes, but it is difficult to obtain films with a well controlled number of layers and size (Supplementary Information section 1.1). CVD-based methods fit the foundry scalable manufacture requirements, but typically do not offer the precise control needed for the growth of uniform wafer-scale single-domain monolayers¹³⁵.

To produce 3D freestanding nanomembranes for vdW integration, various layer lift-off techniques can be deployed²² (Fig. 3b). In chemical lift-off (also called epitaxial lift-off), the 3D films are detached from the substrate by selectively etching a sacrificial interlayer^{136,137}. Laser lift-off leverages optical absorption selectivity and is usually applied with transparent substrates such as GaN for the ablation of an interlayer to delaminate the top material film^{138,139}. Mechanical spalling utilizes a stressor layer to physically peel off a thin layer from the bulk³²; this method is fast but the film thickness and surface roughness are hardly controllable. Smart-cut is another mechanical delamination method of producing thin films for heterogeneous wafer bonding^{50,70}. 2D material-assisted layer transfer is an emergent technique using templates grown by vdW epitaxy¹⁴⁰ or remote epitaxy^{20,23} (Supplementary Information section 1.2); it features fast film release and precisely controlled film thickness, but requires specific sample preparation²⁰. In remote epitaxy²³ nucleation of the template takes place on monolayer (or few-layer) graphene, used as a semitransparent interlayer enabling remote interactions between substrate and adatoms^{43,65}, whereas in vdW epitaxy¹⁴⁰ thick 2D material stacks totally block the influence of the substrate.

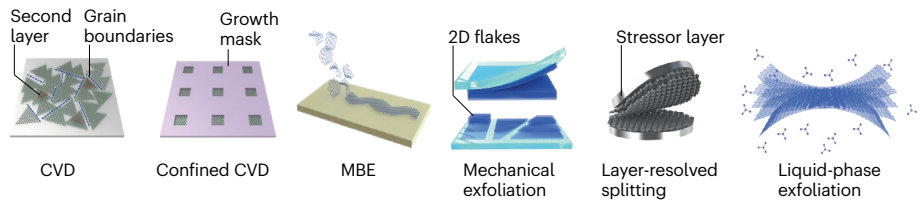
The different methods of preparing 2D and 3D nanomembranes are compared in Fig. 3c. Dry or wet transfer methods (Fig. 3d) can be subsequently used for layer transfer and vdW integration of these 2D and 3D freestanding nanomembranes (Supplementary Information 1.3).

Optical coupling with photonic structures

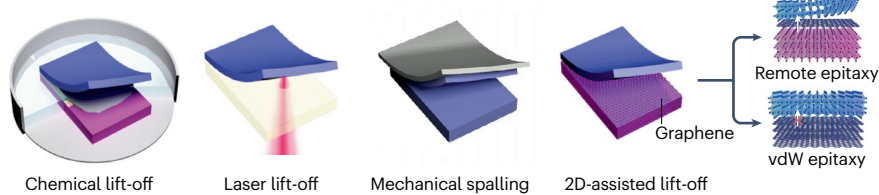
The unique features of 2D materials and 3D freestanding nanomembranes have enabled new functionalities in photonic structures¹. For example, through the vdW integration of functional membranes with optical waveguides, evanescent coupling can take place between two structures⁸². By applying electrical gating or optical pumping, the modification of the properties of the vdW film can modulate the effective mode index ($\tilde{n} = n + ik$) of an underlying waveguide^{56,141}. Changes to the imaginary part k correspond to either optical loss or gain for optical damping or amplification, whereas the real part n modulates the light phase. If anisotropic optical absorption between different polarization states is engineered, integrated polarizers can also be achieved.

vdW films have opened up new opportunities for nonlinear optics, sensing and lasing applications, where light confinement matters and vdW films are used for optical resonators. In a high-quality-factor optical microresonator, photons are trapped in a highly confined volume for a long time owing to the minimized optical loss coming from surface scattering¹⁴². Benefiting from both temporal accumulation and spatial confinement of light, the electromagnetic fields can be densely confined inside the optical cavity with an enhancement factor ranging from hundreds to billions, dramatically enhancing the light–matter

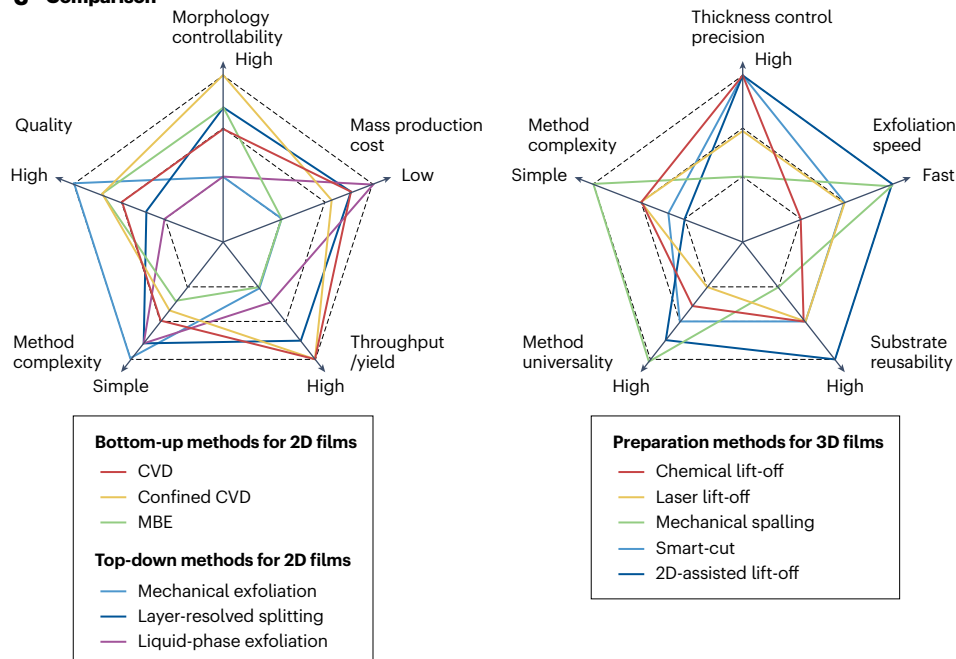
a 2D film preparation



b 3D film preparation



c Comparison



d Film transfer

Dry transfer



Wet transfer

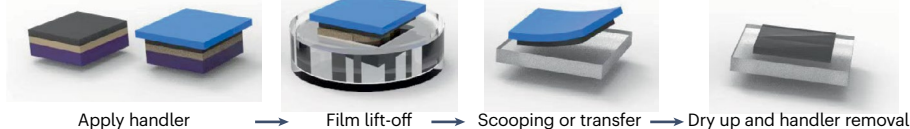


Fig. 3 | Preparation of freestanding optical films. **a**, Methods of preparing 2D films. Confined chemical vapour deposition (CVD) is done on geometrically confined substrates with pre-patterned pockets¹³⁵. **b**, Layer lift-off strategies to obtain 3D freestanding films²². **c**, Comparison of the approaches used to prepare 2D (left) and 3D (right) films in terms of quality, cost, speed and other

properties^{12,22,133,134}. **d**, Elastomeric stamps-based dry transfer method (top)²¹ and polymer handler-based wet transfer method (bottom). MBE, molecular beam epitaxy; vdW, van der Waals. Panel **a** (layer-resolved splitting schematic) modified from ref. 134. © The Authors, some rights reserved; exclusive licensee AAAS.

interaction strength and boosting the performance of optical devices. vdW films for microresonators are selected for specific applications: for example, EO materials for high-speed optical modulation and frequency shifting⁷⁵, piezoelectric materials for light-coupled ultrasound transduction, and MO materials for nonreciprocal devices⁸⁴.

Metasurfaces are made of judiciously engineered subwavelength optical scatterers^{32,33,143} that enable control of the phase, polarization and wavevector of light. vdW films can be optically coupled to metasurfaces, and also to quantum-confined structures like nanowires

and quantum dots¹⁴³. Because these structures can be grown through strain relaxation, it is easy to form highly crystalline structures that are appealing for light-emitting devices owing to their unique quantum-confinement properties.

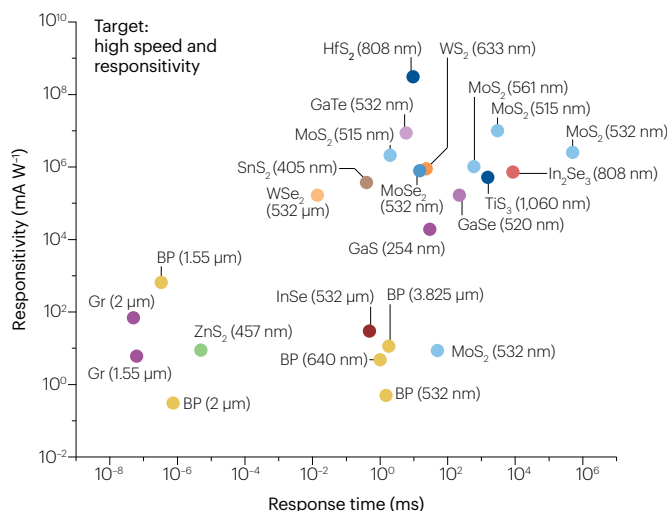
Applications of 2D photonic vdW films

We now outline representative optical applications of 2D vdW films (Fig. 4a), compare their performance in photodetectors coupled with diverse photonic structures (Fig. 4b and Supplementary

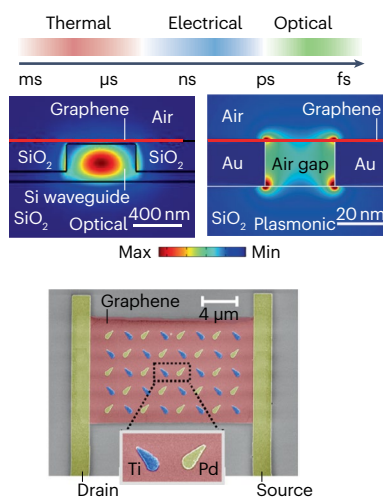
a Functionalities of 2D materials

Semimetallic	Semiconducting	Insulating
HfTe ₂ , TiSe ₂ , TaS ₂ (1T-phase), graphene...	Black phosphorus, transition metal dichalcogenides (MoTe ₂ , MoSe ₂ , WSe ₂ , WS ₂ , ...), α-In ₂ Se ₃ , CrI ₃ , Fe ₃ GeTe ₂ , ...	Ga ₂ N ₃ , h-BN, ...
Topological physics	Optical modulators	Light sources, amplifiers, photodetectors
Plasmonics, surface plasmon polaritons	Exciton polaritons	Ferroelectricity, ferromagnetism, ... Phonon polaritons
	Nonlinear optics	

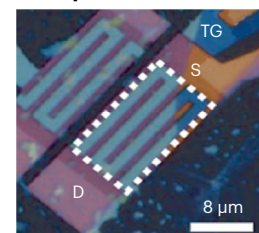
b 2D-materials-based photodetectors



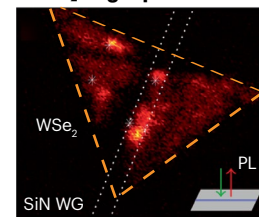
c Photonic applications of graphene



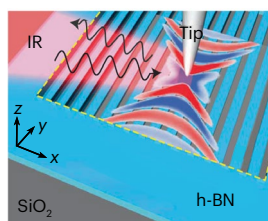
d BP spectrometer



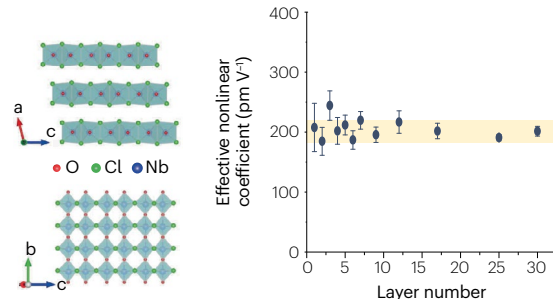
e WSe₂ single-photon emitter



f h-BN metasurface



g Nonlinear susceptibility in NbOCl₂



h Applications of quasi-2D halide perovskites

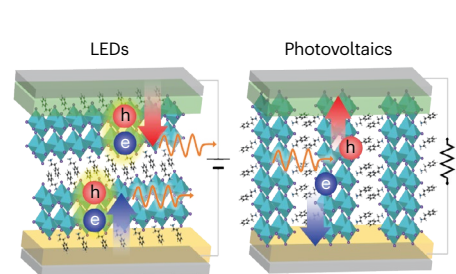


Fig. 4 | Applications of 2D photonic vdW films. **a**, Functionalities of 2D van der Waals (vdW) nanomembranes^{13,14,63,64,167}. **b**, Comparison of various 2D-materials-based photodetectors^{16,91,157} (the operation wavelengths are marked beside the materials labels). **c**, Graphene photonic applications. Optical modulation schemes for graphene (top)⁵⁶, graphene optical¹⁵³ and plasmonic modulators¹⁵³ (middle) enabled by integrating graphene with Si and gold waveguides, respectively, via vdW interactions, and a graphene-assisted metasurface polarization detector (bottom)¹⁵⁵. **d**, Black phosphorus (BP) spectrometer with source (S), drain (D) and top-gate (TG) electrodes¹⁶⁹. **e**, Single-photon emitter fabricated by vdW integration of WSe₂ on an optical waveguide (WG)¹⁷⁷. The inset shows the confocal photoluminescence (PL) measurement setup: the excitation beam and PL are

injected and collected from the top, respectively. **f**, h-BN hyperbolic metasurface for hyperbolic phonon polaritons with exotic wavefronts¹⁵⁰. **g**, NbOCl₂ crystal structure (left) and layer-independent effective nonlinear coefficient (right)⁵⁷. Vertical error bars denote standard deviation. **h**, Representative applications of quasi-2D halide perovskites: light-emitting diodes (LEDs) and photovoltaic devices. h-BN, hexagonal boron nitride; IR, infrared. Panel **c** (optical modulator) adapted from ref. 151, Springer Nature Limited. Panel **c** (plasmonic modulator) adapted from ref. 153, Springer Nature Limited. Panel **c** (metasurface) adapted from ref. 155, Springer Nature Limited. Panel **d** adapted from ref. 169, Springer Nature Limited. Panel **e** adapted from ref. 177, CC BY 4.0. Panel **f** adapted with permission from ref. 180, AAAS. Panel **g** adapted from ref. 57, Springer Nature Limited.

Information section 2), and highlight emergent 2D photonic materials with unconventional characteristics such as quasi-2D halide perovskites^{103,144}.

2D semimetals

Owing to its unique band structure, graphene exhibits high carrier mobility, wideband optical transparency, gate-tuneable optical transitions⁸⁷, giant optical nonlinearity¹⁴⁵ and tuneable surface plasmons¹⁴⁶, properties that make it a versatile platform for numerous photonic applications, including on-chip information processing, optical communications, imaging and biosensing^{47,49,133}.

By evanescently coupling graphene with the guided modes inside optical waveguides, diverse integrated modulators can be prototyped for photonic integrated circuits (Fig. 4c, top), such as EO^{147–149}, TO¹⁵⁰ and all-optical¹⁴² modulators (Fig. 4c, middle), working either in the optical^{84,141,151} or plasmonic regime^{152,153}. Graphene can be also integrated with optical fibres, photonic crystals and metasurfaces^{143,154–156} for signal processing and broadband photodetection^{16,91,97,157,158} (Fig. 4b and Supplementary Information 2). For instance, graphene with ultrafast photoresponse was integrated with a metasurface with broken in-plane inversion symmetry for direct photodetection of light polarization¹⁵⁵ (Fig. 4c, bottom).

Graphene also enables widely tuneable optical nonlinearity from infrared to terahertz wavelengths⁴⁵ when integrated with gated metal nanostructures^{145,159} to funnel light into small volumes. Tuneable frequency combs¹⁶⁰ and other nonlinear applications¹⁵⁹ are also feasible. Furthermore, graphene can be patterned into specific shapes to realize nano-resonators^{161,162}, transformation optics¹⁶³, meta-optics^{32,33} and near-field nano-imaging^{164,165}.

Other 2D materials such as NbSe₂, Ta₂Se₃, β -BiO₂ (refs. 166,167) and some transition metal trichlorides can also be engineered to exhibit semimetal states for studying condensed matter physics and topological photonics.

2D semiconductors

Despite the exceptional broadband photo-responsivity of graphene, graphene photodetectors have the drawbacks of a relatively high dark current and noise owing to the lack of an electronic bandgap⁹¹. Other 2D materials such as BP and TMDs have better performance for active photonic devices such as photodetectors (Fig. 4b), amplifiers and light sources^{16,168}. In particular, BP photodetectors fabricated by vdW integration feature widely configurable operational wavelengths from the ultraviolet to the mid-infrared range¹⁵⁸. The strong in-plane anisotropy, optical dichroism and tuneable absorptive response of BP can also be exploited by vdW integration of BP for ultracompact chip-integrated spectrometers¹⁶⁹ (Fig. 4d), optical polarizers¹⁷⁰, modulators¹⁷¹ and in bio-sensing applications²⁶.

2D TMD monolayers with direct bandgap (1–2 eV) and strong spin-orbit coupling are prominent candidates for exciton physics⁴⁶. By patterning WS₂ film into a metasurface¹⁷², atomically thin meta-lenses can be devised with a focusing efficiency that is electrically configurable by tuning the exciton resonances. Optical modulators can also be designed by integrating, for example, 2D WS₂ or MoS₂ films with photonic waveguides and applying electrical gating⁵⁶ or optical pumping¹⁷³.

Thanks to their direct electronic bandgaps, 2D TMDs are powerful candidates for active optical applications¹⁷². TMD monolayers are also used in a vast range of photodetectors (Fig. 4b) and LEDs. vdW integration of TMD films having optical cavities such as microdisks, photonic crystals and nanobeam resonators to enhance light–matter

interactions¹⁷⁴ results in high optical gain for use in amplifiers¹⁷⁵, nano-lasers¹⁷⁶ and on-chip single-photon emitters¹⁷⁷ (Fig. 4e).

2D insulators

h-BN, with its indirect wide bandgap approaching 6 eV, was originally used as the optimal material to encapsulate graphene to maintain its high carrier mobility and plasmon lifetime^{148,178}. h-BN is also a naturally hyperbolic material at infrared wavelengths, with greatly confined sub-diffractive phonon polaritons that can be used for hyperlensing¹⁷⁹ and bio-imaging¹⁷⁸. h-BN metasurfaces can host in-plane hyperbolic phonon polaritons (which have an anisotropic permittivity, with components with opposite sign along orthogonal axes, and can realize ultrahigh light confinement) tailored by geometric patterning of the h-BN¹⁸⁰ (Fig. 4f).

h-BN can also be integrated with optical cavities to harvest single-photon emission from its defects; the single-photon emission has high stability, brightness and photon energies that reach into the ultraviolet regime¹⁸¹. Inversion-symmetry-broken h-BN bilayers also enable efficient second-harmonic generation¹⁸².

Emergent 2D vdW films

A major limitation of 2D films is that their atomic thickness constrains the light–matter interaction strength. Moreover, the nonlinear optical response does not scale with layer thickness owing to the recovery of centrosymmetry in even-layer and bulky samples of h-BN and TMDs. Recently, NbOX₂ (where X is Cl, Br or I) has been introduced as a new class of vdW materials with vanishing interlayer electronic coupling and layer-independent bandgap⁵⁷. NbOCl₂ shows an intriguing thickness-independent bandgap of around 1.6 eV with a preserved non-centrosymmetric structure, yielding a layer-independent nonlinear susceptibility of around 200 pm V⁻¹ (ref. 57) (Fig. 4g). An absolute second-harmonic generation conversion efficiency of over 0.2% was demonstrated in strained NbOI₂ (ref. 58). The unique independence of the nonlinear susceptibility on the number of layers in NbOX₂ means that the second-harmonic generation intensity and power conversion efficiency both scale quadratically with the number of layers, enabling the extension of classical harmonic generation to correlated photon-pair generation via spontaneous parametric downconversion in the quantum regime.

Photonic applications of 2D MXenes, which typically display indirect bandgaps, include saturable absorbers and nonlinear optics. Quasi-2D halide perovskites, which are cubic or orthorhombic crystal systems with direct bandgaps, can be used in LEDs, photovoltaic devices and photodetectors^{102,103} (Fig. 4h). More details about 2D MXenes and quasi-2D perovskites are provided in Supplementary Information section 3.

Applications of 3D photonic freestanding films

Freestanding 3D nanomembranes can be derived from arbitrary bulk crystals via various layer lift-off techniques^{21,23}, and thus offer a wide range of lattice structures and optical functionalities²⁰. Thanks to their vdW interfaces¹¹, they are easy to integrate and couple with various photonic structures, opening up opportunities for the fabrication of previously unachievable hetero-integrated devices²⁰.

Currently available 3D freestanding vdW building blocks for photonic vdW integration^{21–23} encompass a vast range of materials with disparate lattice structures and optoelectronic responses^{8,41,43,183–188} (Fig. 5a and Supplementary Table 1). In this section, we outline photonic and optoelectronic applications underpinned by the vdW integration of freestanding 3D films.

Review article

Metal films

Freestanding metal films²² are used as optical media for surface plasmons and vdW electrical contacts, which offer reduced surface disorder and contact resistance compared with conventional deposited electrodes¹¹⁴. A graphene-assisted transfer technique (Fig. 5b) can be used to obtain wafer-scale vdW metal contacts without dangling bonds and with engineerable Ohmic to Schottky contacts, even for strongly adhesive metals such as Pt, Ti and Ni¹⁷⁹.

VdW integration of various metal films enables the investigation of the optical coupling between surface plasmon polaritons with photonic structures to tailor their propagation and dispersion. For instance, a metal–dielectric–metal nanogap plasmonic waveguide formed by two ultrathin gold flakes was used to study nonlocal surface plasmon polariton effects¹⁸⁹ (Fig. 5c). The vdW metallic nanomembranes can also be used to fabricate self-assembled Fabry–Pérot optical microcavities in an aqueous solution to study the tuneable interplay between the Casimir and electrostatic forces¹⁹⁰.

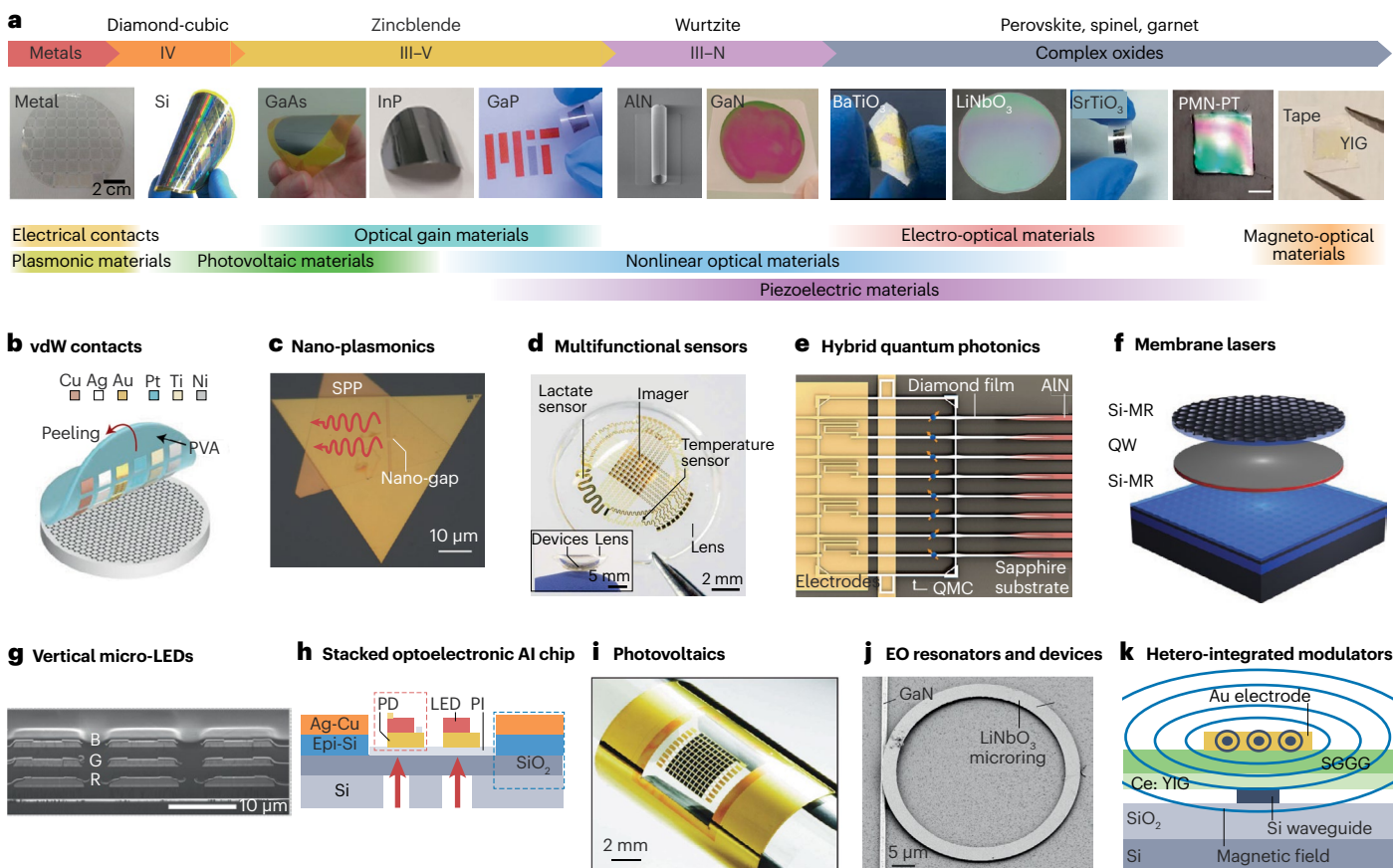


Fig. 5 | Applications of 3D photonic vdW films. **a**, Functionalities of freestanding 3D nanomembranes for photonic van der Waals (vdW) integration. Metal foils on poly-vinyl acetate (PVA)¹⁷⁹, a Si film¹⁸³, GaAs¹⁸⁴, InP¹⁸⁵, GaP⁴³, AlN¹⁸⁶, GaN⁴¹, BaTiO₃ (ref. 188), LiNbO₃ (refs. 187,224), SrTiO₃ (ref. 8), lead magnesium niobate-lead titanate (PMN-PT)⁸ and yttrium iron garnet (YIG)⁸. **b**, Graphene-assisted metal-foil transfer¹⁷⁹. **c**, Transferred metal flakes used to study surface plasmon polaritons (SPPs)¹⁸⁹. **d**, Multifunctional lens detector and sensor¹⁹⁴. **e**, Hybrid diamond quantum emitter-photonics chip¹⁹⁹. **f**, Membrane laser fabricated by transferring InGaAsP quantum wells (QWs) on Si nanomembranes acting as membrane reflectors (MRs)²⁰⁹. **g**, Vertical full-colour micro light-emitting diodes (LEDs) made by 2D-material-assisted layer transfer of stacked nanomembranes emitting red (R), green (G) and blue (B) light²¹¹. **h**, Stackable hetero-integrated optoelectronic chip combining light emission through a LED layer, detection through a photodetector (PD) layer and neuromorphic computing³⁶. The optoelectronic device stack is highlighted in red, the neuromorphic computing core in blue. The red arrows represent the vertical light emission path. **i**, Flexible GaAs solar cell array on a polyethylene terephthalate substrate²¹². **j**, Scanning electron microscope image of a LiNbO₃ ring resonator on GaN waveguide²²³. **k**, Integrated magneto-optical modulator fabricated by

transferring substituted gadolinium gallium garnet (SGGG)/Cd-doped YIG onto a Si waveguide. EO, electro-optical; Epi, epitaxial; PI, polyimide; QMC, quantum microchiplet. Panel **a** (metal films) reprinted from ref. 179, Springer Nature Limited. Panel **a** (Si) reprinted with permission from ref. 183. Copyright 2013 American Chemical Society. Panel **a** (GaAs) reprinted from ref. 184, Springer Nature Limited. Panel **a** (InP) reprinted with permission from ref. 185. Copyright 2020 American Chemical Society. Panel **a** (GaP) reprinted from ref. 43, Springer Nature Limited. Panel **a** (AlN) reprinted with permission from ref. 186. Copyright 2022 American Chemical Society. Panel **a** (BaTiO₃) reprinted from ref. 188, CC BY 4.0. Panel **a** (LiNbO₃) reprinted with permission from ref. 187, Wiley. Panel **a** (SrTiO₃, PMN-PT and YIG) reprinted from ref. 8, Springer Nature Limited. Panel **a** (GaN) reprinted from ref. 41, Springer Nature Limited. Panel **b** adapted from ref. 179, Springer Nature Limited. Panel **c** adapted from ref. 189, CC BY 4.0. Panel **d** adapted from ref. 194, Springer Nature Limited. Panel **e** adapted from ref. 199, Springer Nature Limited. Panel **f** reprinted from ref. 209, Springer Nature Limited. Panel **g** reprinted from ref. 211, Springer Nature Limited. Panel **h** reprinted from ref. 36, Springer Nature Limited. Panel **i** adapted from ref. 212, Springer Nature Limited. Panel **j** reprinted with permission from ref. 223, IEEE. Panel **k** reprinted from ref. 85, CC BY 4.0.

Semiconductors

The distinctive optoelectronic properties of semiconductors make them ideal platforms for applications including light generation, manipulation and detection². Semiconductors comprise optical gain, nonlinear, photovoltaic and piezoelectric materials (Fig. 5a). Recent endeavours have used various freestanding semiconductor nanomembranes as innovative playgrounds in which to prototype novel applications via vdW integration with prefabricated photonic architectures (Supplementary Table 1).

Group IV nanomembranes. Freestanding Si films with diamond-cubic lattices have good photoresponsivity and photovoltaic properties^{183,191}. When a thin layer of crystalline Si is delaminated from the substrate²², its stiffness is drastically reduced, enabling flexible optical applications²⁰. For instance, Si nanomembranes integrated with metal interconnects can be attached to 3D curved optical templates to make biomimetic electronic eye cameras^{192,193}. These devices, being organized along a 3D hemisphere that imitates the remarkable imaging system of human eyes¹⁹², feature low aberration and a wide field of view. Novel multifunctional optical systems are also made possible by the vdW integration of multiple functional layers. For example, a multifunctional contact lens has been developed that can simultaneously image and act as sensors for both temperature and lactate for wearable optoelectronic applications¹⁹⁴ (Fig. 5d). Moreover, Si films resting on stretchable substrates can be used in flexible solar cells (though with slightly lower efficiency than traditional cells because of additional processing)^{116,117}, offering a material-saving strategy to reduce installation costs¹¹⁸.

Besides Si, diamond-based and Ge-based vdW films are also used in photonic applications. Diamond, as a form of highly crystallized carbon, features a wide bandgap and optical transparency from the infrared to the deep-ultraviolet range¹⁹⁵. More importantly, diamonds can contain colour centres (optically active defects) that hold promise for quantum photonic applications as single-photon sources³⁴. vdW integration can enable various novel architectures through the coupling of diamond films with waveguides and optical cavities^{196–198}. For example, in a hybrid integrated photonic chip, diamond films with optically addressable colour centres were transferred onto aluminium nitride (AlN) waveguides¹⁹⁹ (Fig. 5e). This heterostructure combines the photonic properties of both materials: the excellent linear and nonlinear waveguiding properties of AlN and the controllable transitions of single-photon emitters in diamond-based films. Ge membranes can be used to develop high-performance infrared photodetectors^{200,201} and stretchable LEDs^{202,203}.

III–V nanomembranes. III–V semiconductors feature outstanding optoelectronic properties, including widely engineerable bandgaps, high carrier mobility, good optical gain, nonlinearity and good photovoltaic properties²⁵. These materials form a homologous series of compounds with zincblende or wurtzite crystal structure. Representative binary semiconductors, such as GaAs, InAs, InP, GaN and AlSb, possess direct bandgaps that enable efficient absorption and emission of light²⁵, and are thus promising materials for thin-film devices for interaction with light.

The vdW integration with high-quality III–V nanomembranes can substantially broaden the scope of Si and SiN photonics^{21,24} by enabling high-performance on-chip lasers^{204,205}, optical amplifiers²⁰⁶ and photodetectors^{207,208} from the visible to the mid-infrared range, which are challenging to realize in pure Si platforms. Single-crystalline III–V thin films acting as gain media can be conveniently integrated with foreign

substrates with prefabricated photonic structures with a clean and disorder-free interface, which is crucial for LEDs, lasing and photovoltaic applications. For example, a hetero-integrated vertical-cavity surface-emitting laser²⁰⁹ was fabricated by transferring and stacking InGaAsP quantum wells, acting as the gain medium, on patterned Si nanomembranes, and as the membrane reflector (Fig. 5f). Besides transferring individual III–V nanomembranes to build integrated photonic devices, whole devices can also be transferred to fabricate vdW-integrated optical systems^{24,119}.

Freestanding III–V films not only enable novel hetero-integrated photonic devices with excellent performance^{21,24}, they may also drastically reduce the cost of substrates for non-Si materials^{204,205}. For example, in red LEDs based on AlGaAs films and fabricated by remote epitaxy⁴², a Ge substrate coated with nanopatterned graphene was used to minimize the number of heteroepitaxial defects in GaAs, acting as a potentially recyclable template for low-cost single-crystal nanomembranes²¹⁰. Moreover, the ultrathin and freestanding nature of the isolated 3D III–V membranes facilitates novel vertical-integration architectures for compact multifunctional optoelectronic systems³⁵. For instance, full-colour micro-LEDs were fabricated by vertically stacking III–V nanomembranes emitting red, green and blue light, greatly enhancing the pixel density²¹¹ (Fig. 5g). In an exemplary 3D hetero-integrated chip, different functional layers – a light-emitting layer based on InGaP, a photodetection layer based on GaAs and a neuromorphic computing core based on an Ag-Cu-alloy and on Si – were stacked together like Lego bricks³⁶ (Fig. 5h). This system can directly recognize input letter images thanks to its unparalleled interlayer communications and excellent parallel data-processing capabilities.

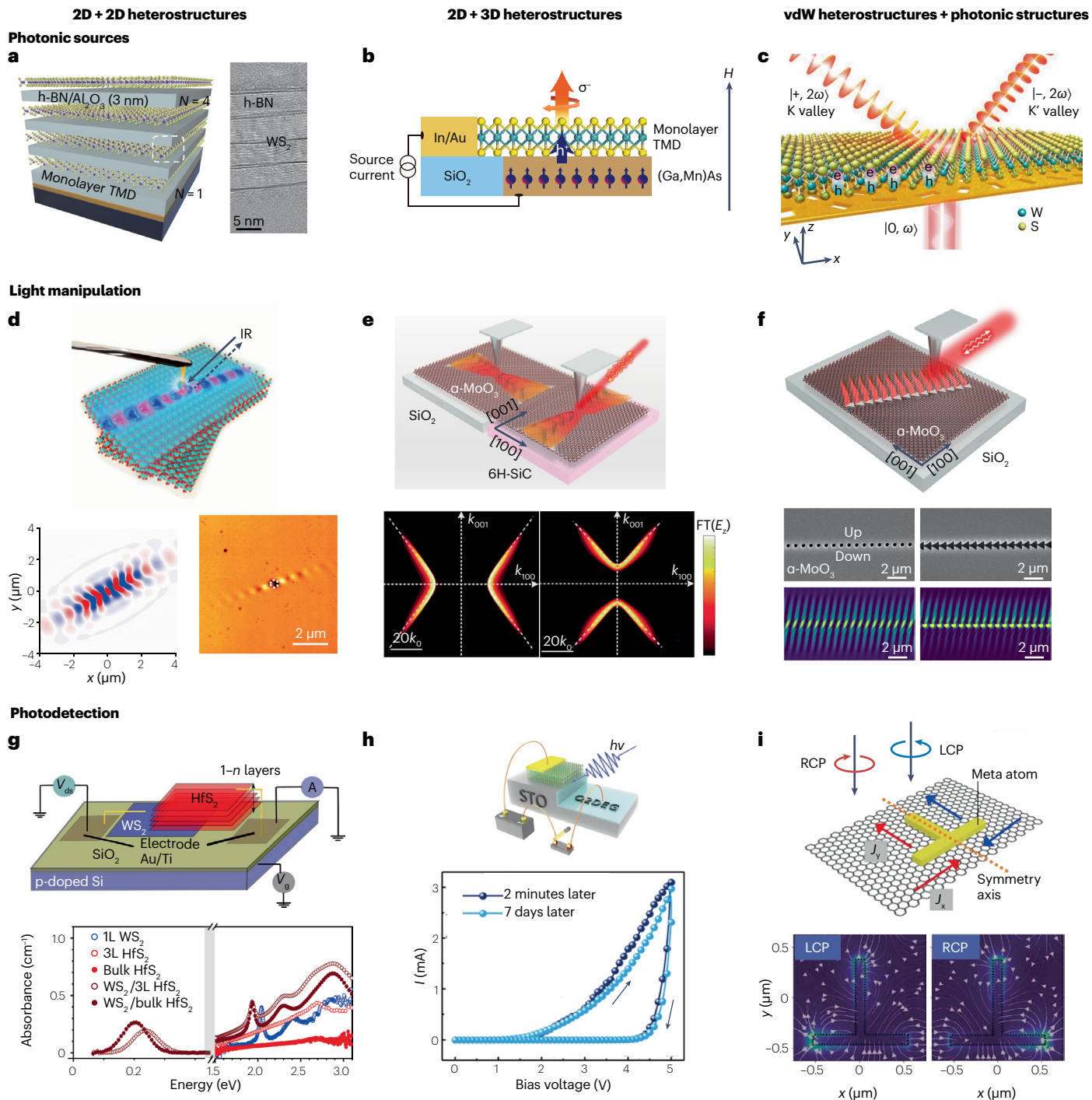
Freestanding III–V semiconductors can be also used in ultrathin solar cells, offering advantages that include reduced material cost, enhanced solar energy conversion and enhanced carrier collection. GaAs-based solar cells are the most established. Compared with Si, GaAs thin-film solar cells are advantageous for their direct bandgap, high efficiency and flexibility²¹² (Fig. 5i).

Wide-bandgap III–nitride membranes such as AlN and GaN with different thicknesses²¹³ are useful for blue-light micro-LEDs, lasers and photodetectors²¹⁴. The piezoelectricity of III–nitride nanomembranes can be leveraged to exploit optomechanical effects and optical modulations by integrating them with microcavities and waveguides for photonic applications, including optical frequency converters, piezoelectric optical modulators, actuators and quantum photonic devices^{215–218}. Optical applications of other freestanding semiconductor nanomembranes made of II–VI and IV–VI materials are discussed in Supplementary Information section 4.

Freestanding oxide crystals

Complex oxides are widely used in photonic applications because they comprise nonlinear optical crystals that include EO materials (such as LNO, BaTiO₃ and SrTiO₃)^{70,219} and MO materials (such as the garnet Y₃Fe₅O₁₂, YIG)²²⁰. Oxide crystals with perovskite structure have attracted particular interest owing to their ferroelectricity and piezoelectricity, which can be used in applications that include light modulation, sensing, nonlinear frequency generation, optomechanical coupling and metrology^{8,220}. Freestanding nanomembranes of these materials are thus an ideal platform for hetero-integrated photonic systems that exploit the interplay between light and other physical fields such as mechanical strain and electric and magnetic fields²⁰.

Review article



EO nanomembranes. Before the advent of smart-cut techniques, the integration of single-crystalline EO thin films with optical substrates was challenging owing to drastic epitaxial lattice mismatches⁷⁰. Now, ion-sliced LNO membranes attached to SiO₂ substrates (using direct wafer bonding or adhesive polymers such as benzocyclobutene) provide an ‘LNO-on-insulator’ photonic platform for diverse EO and nonlinear applications^{70,187}. High-performance chip-integrated EO modulators^{30,71,72}, spectrometers⁷⁷, second-harmonic generators, frequency combs and shifters^{69,75,76} can be realized in electrically gated

LNO waveguides and resonators⁷⁴. On-chip interactions between electromagnetic waves and mechanical vibrations like acoustic waves can also be exploited^{142,221,222}.

Besides wafer bonding, smart-cut LNO films can also be patterned and transferred for vdW integration with prefabricated photonic structures. For instance, LNO EO resonators were positioned on a GaN waveguide for nonlinear optical applications²²³ (Fig. 5j). This approach does not require substrate flatness and enables the fabrication of both laterally and vertically stacked optical structures. Other freestanding EO

Fig. 6 | Photonic applications of vdW heterostructures. Photonic functionalities enabled by constructing 2D–2D, 2D–3D and van der Waals (vdW)-nanophotonic heterostructures. **a–c**, Photonic sources. **a**, Schematic illustration and scanning electron microscope image of a 2D superlattice formed by the layer-by-layer assembly of 2D monolayers and insulating spacers²³¹. The dashed white box highlights one unit cell. **b**, Schematic of a transition metal dichalcogenide (TMD)/(Ga,Mn)As heterostructure for valley polarized electroluminescence. **c**, Au–WS₂ metasurface that steers nonlinear valley photons²⁴⁰. **d–f**, Light manipulation. **d**, Twisted bilayer α -MoO₃ enables the manipulation of polariton propagation (top). Simulated and measured near-field distribution of canalized polariton propagation (bottom)⁶⁰. **e**, Schematic (top) and dispersion (bottom) of polariton propagation in an α -MoO₃/SiO₂ and in an α -MoO₃/SiC heterostructure²⁴⁸. **f**, Scheme and scanning electron microscope images and simulated near-field distributions for α -MoO₃ sample with a circular hole (left) and blazed (right) diffraction grating⁶¹. **g–i**, Photodetection. **g**, Schematic (top) and absorbance spectra (bottom) of an infrared photodetector enabled by interlayer excitons in 2D–2D heterostructures²⁵³. 1L and 3L indicate 1 and

3 monolayers. **h**, Schematic illustration of photoelectric conversion and storage in a WS₂/quasi-2D electron gas (Q2DEG) heterostructure (top). Current–voltage (I – V) curves measured in darkness 2 minutes and 7 days after illumination ($h\nu$)²⁵⁷. **i**, Vectorial photocurrents in an achiral plasmonic nanostructure-on-graphene heterostructure (top). Simulated near-field profiles for left- and right-handed circularly polarized light (LCP and RCP, respectively) illumination (bottom)²⁵⁹. FT(E_z), Fourier transform of electric field component at vertical z direction; IR, infrared; STO, SrTiO₃. Panel **a** reprinted from ref. 231, Springer Nature Limited. Panel **b** reprinted with permission from ref. 236, Springer Nature Limited. Panel **c** reprinted from ref. 240, Springer Nature Limited. Panel **d** reprinted from ref. 60, Springer Nature Limited. Panel **e** reprinted with permission from ref. 248. Copyright 2021 American Chemical Society. Panel **f** reprinted with permission of AAAS from ref. 61. © The Authors, some rights reserved; exclusive licensee AAAS. Distributed under a CC BY-NC 4.0 License (<http://creativecommons.org/licenses/by-nc/4.0/>). Panel **g** reprinted from ref. 253, Springer Nature Limited. Panel **h** reprinted with permission from ref. 257, APS. Panel **i** reprinted from ref. 259, Springer Nature Limited.

oxides, such as highly crystalline SrTiO₃ and BaTiO₃ nanomembranes, were also recently reported^{8,154,188,219,224} as promising alternatives to enable diverse EO applications²³.

MO nanomembranes. YIG and terbium iron garnet (TIG) are used in non-reciprocal optical devices such as optical isolators, circulators and magnetic-field sensors^{220,225}. Compared with directly deposited garnets⁸⁴, vdW-integrated MO nanomembranes have better crystallinity, because the freestanding garnet films are prepared on suitable parent substrates and then transferred to target optical structures for applications²². For example, an MO modulator made of a transferred Ce:YIG layer bonded to an underlying Si resonator (Fig. 5k) was used to develop superconducting circuits with high operation speed⁸⁵. The MO effect was effectively induced via patterned metal coil electrodes on top of the YIG film, and high data rates of up to 2 Gb s⁻¹ with low power consumption were demonstrated. Other spinel MO nanomembranes like CoFe₂O₄ can also be integrated with photonic structures via vdW interactions to explore physical fields coupling and non-reciprocal optical applications^{8,226}.

Piezoelectric nanomembranes. Photo-sensing and luminescent devices can be stacked in vdW heterostructures with oxide piezoelectric nanomembranes and active device materials to investigate strain-modulated physical fields²²⁷. For instance, in a Mn:ZnS and Pb(Mg_{1/3}Nb_{2/3})O_{3-x}PbTiO₃ (PMN-PT) heterostructure, strain can be induced by applying a bias voltage to the PMN-PT layer to change its potential and effectively tune its band structure, affecting the charge transport in ZnS²²⁸. Compared with direct heteroepitaxial structures, vdW integration mitigates grain boundary and defects issues that previously hindered device performance.

Photonic applications of vdW heterostructures

Thanks to the vdW interfaces of these freestanding nanomembranes, various vdW heterostructures (2D, 3D and hybrid) with strong interlayer coupling can be fabricated. These heterostructures host intriguing phenomena, such as exotic interlayer excitons and moiré flatbands^{1,129}. Besides 2D–2D heterostructures^{9,12–14}, we also discuss emergent 2D–3D hybrid heterostructures, highlighting their varied properties and enhanced light–matter interactions. We also survey the integration of vdW heterostructures with artificial photonic structures with designable electromagnetic properties

including the enhanced generation, manipulation and detection of photons.

vdW photonic sources

By integrating TMD monolayers into vdW heterostructures, on-chip ultracompact photonic sources can be developed. The spin–valley locking in the bandstructure of these heterostructures enables electrically tuneable circularly polarized photoluminescence (PL)²²⁹, electroluminescence (EL)²³⁰, single-photon emission¹⁷⁷ and nonlinear harmonic generation¹⁷⁵. The layer-by-layer vdW stacking of 2D TMD monolayers and insulating spacers (such as h-BN and Al₂O₃; Fig. 6a) is an effective way of preventing electronic coupling between TMD monolayers and harvesting their tightly bound excitons for photonic sources²³¹. In such a superlattice the direct bandgap, exciton resonance and strong luminescence are maintained. Both excitonic absorption and PL scale with the TMD layer number. Greatly enhanced light–matter interactions are reflected by the observation of exciton polaritons: quasi-particles formed by strong coupling of excitons and photons. This multilayer vdW superlattice supports exciton polaritons without a high-quality-factor artificial microcavity, opening up opportunities for the enhancement of nonlinear optical effects, such as spontaneous parametric downconversion⁵⁷ and optical parametric amplification¹⁷⁵.

The twist angle is another parameter that can be used to explore vdW polaritons. Moiré superlattices formed in twisted TMD bilayers host flatbands that result in strongly correlated exciton physics^{128,132} and strong light–matter interactions.

Complex 3D materials and their epitaxial heterostructures represent a versatile platform on which to host ferroelectricity, magnetism, magneto-electric coupling and superconductivity²³². Exploiting the variety of properties and strong light–matter interactions of 3D nanomembranes, 2D–3D heterostructures have been developed to control light emission. First, 3D materials with giant and switchable ferroelectric polarization have been integrated with TMDs for manipulating light emission²³³, carrier dynamics²³⁴ and harmonic generation²³⁵. The electrostatic doping of TMDs can be controlled by the ferroelectric polarization in LiNbO₃, giving rise to modulated PL emission in the TMDs²³³. Beyond linear optics, interfacing TMDs with 3D ferroelectrics also enables the modulation of second-harmonic generation by polar symmetry at domain walls²³⁵. Second, 3D ferromagnets have been introduced for spin injection and breaking of time-reversal symmetry. For instance, a heterostructure made of n-type WS₂ and p-doped (Ga,Mn)

As sustains circularly polarized EL²³⁶ (Fig. 6b). Such spin-polarized EL is realized by spin injection from the diluted ferromagnetic semiconductor (Ga,Mn)As, which populates spin-polarized holes at the K and K' valleys of WS₂ in a way that can be controlled by magnetic field. Electrical injection of spin-polarized carriers has also been obtained through tunnelling from the vdW ferromagnetic metal Fe₃GeTe₂ to WSe₂ (ref. 237). Breaking the energy degeneracy of valley pseudospins is pivotal in valleytronics, but valley energy splitting is tiny for TMD monolayers under an applied magnetic field. In 2D-semiconductor/3D-ferromagnet (WSe₂/EuS) heterostructures, an enhanced valley energy splitting of 2.5 meV at 1 T was demonstrated via interfacial magnetic exchange field, corresponding to an effective magnetic exchange field of about 12 T (ref. 238). This valley energy splitting can be further enhanced to 16 meV T⁻¹ by exploiting the magnetic proximity effect in these heterostructures²³⁹.

Photonic structures can also be integrated with 2D and 3D vdW heterostructures for enhancing light–matter interactions and controlling the properties of the emitted light, such as polarization, momentum and phase. For example, leveraging spin-related Pancharatnam–Berry phase metasurfaces^{32,33,143}, left and right circularly polarized light can be deflected in opposite directions²⁴⁰. This geometric phase concept can be combined with second-order nonlinear optical selection rules in TMD monolayers, for which second-harmonic waves with opposite helicity are generated from circularly polarized fundamental waves. In an heterostructure combining WS₂ with a Au metasurface with geometric phase, second-harmonic nonlinear photons can be steered with opposite diffraction angle under circularly polarized pumping²⁴⁰ (Fig. 6c). This concept is extendable to the generation and steering of second-harmonic vortex beams with tuneable orbital angular momentum²⁴¹. The on-chip generation and routing of valley chiral photons can also be supported by spin-dependent beating patterns in a waveguide integrated with a TMD monolayer²⁴².

vdW light manipulation

Manipulation of light propagation at the deep subwavelength scale is pivotal to integrated photonics³. vdW heterostructures are ideal platforms for the realization of vdW polaritons formed by strong light–matter coupling²⁴³. These quasiparticles can confine light at deep subwavelength length scales.

Orthorhombic α -MoO₃, a polar vdW crystal with strong in-plane anisotropy, has emerged as a good platform for hosting hyperbolic polaritons^{1,59}. Hyperbolic polaritons are quasi-particles formed by light–matter coupling in hyperbolic materials, which exhibit extremely anisotropic permittivity with opposite sign in orthogonal directions⁵⁹. The polariton dispersion can be steered in twisted vdW homobilayers of α -MoO₃ (ref. 60) (Fig. 6d, top). By changing the twist angle, the polariton dispersion gradually transitions from hyperbolic to elliptical, owing to the conservation of a topological invariant: the number of anti-crossing points in the dispersion lines of the two α -MoO₃ layers. At a critical twist angle, the polariton dispersion transforms from closed to open, and a flattened dispersion forms, causing polaritons to propagate directionally without diffraction (Fig. 6d, bottom). This twist strategy is also applicable to other quasiparticles for dispersion engineering. For instance, in nanostructured graphene bilayers with hyperbolic dispersion, moiré plasmons with field canalization and low damping can be achieved by tuning the twist angle between the layers²⁴⁴.

In graphene/h-BN vdW heterostructures it is possible to increase the diffusion length of hyperbolic plasmon–phonon polaritons by 1.5–2.0 times and to tune their wavelength by changing the Fermi

energy of graphene via electrostatic gating²⁴⁵. The hybridization of phonon polaritons in α -MoO₃ with surface plasmons in graphene was exploited to create surface plasmon–phonon polaritons, which can be used for the dynamic control of topological transitions in the polariton dispersion²⁴⁶. Above a critical plasmon density, plasmon–phonon hybridization causes the transition of the isofrequency contour from a hyperbole to a closed curve, indicative of the topological transition, which is electrically tuneable.

2D/3D freestanding films offer further opportunities for controlling polariton dispersion and propagation behaviours. Ultraconfined surface phonon polaritons were realized by integrating monolayer TMDs with a polar 6H-SiC layer with negative permittivity²⁴⁷. The ultrahigh squeezing of the surface phonon polaritons is manifested in a wavelength 190 times shorter than that of free-space light with isotropic in-plane propagation. Interfacing α -MoO₃ with polar 6H-SiC can generate in-plane hyperbolic surface phonon polariton modes that propagate in the direction orthogonal to that of phonon polaritons in pure α -MoO₃ (ref. 248) (Fig. 6e). Heterostructures combining vdW films and phase-change materials with tuneable permittivity open up a way to realize rewritable polariton devices, such as a switch made using Ge₃Sb₂Te₆ sandwiched between dielectric layers. The substantial difference in the permittivity of Ge₃Sb₂Te₆ in the crystalline and amorphous state enables rewritable structures that can confine and guide polariton waves²⁴⁹. The nanoscale control of permittivity can also be attained by using Mott transitions between strongly correlated states in phase-change materials like VO₂ and SmNiO₃ (ref. 250).

Aside from the exploration of unusual polariton dispersions in natural materials, artificial photonic structures can be used to manipulate polariton propagation. For instance, h-BN possesses in-plane isotropic and negative permittivity and out-of-plane positive permittivity, yielding out-of-plane hyperbolic phonon polaritons¹⁸⁰. This situation can be altered by breaking the in-plane symmetry with a grating structure with different effective permittivity along three directions, which induces in-plane hyperbolic phonon polaritons. Nanostructures were also used in α -MoO₃ for breaking the symmetric phonon polariton propagation⁶¹ (Fig. 6f). By using a periodic blazed grating aligned with the optical axis of the crystal, unidirectional phonon polariton propagation was realized.

vdW photodetection

The strong light–matter interactions and high carrier mobility of vdW heterostructures make them suitable for photodetectors with high sensitivity and high speed^{12,46}. Single-component photodetectors often present trade-offs between response speed, responsivity and detectivity⁹¹. By contrast, a photodetector based on a vdW heterostructure using graphene for electron extraction and an atomically thin WSe₂ channel for optical absorption and carrier generation combines a high response time of 5.5 ps with an internal quantum efficiency of over 70%²⁵¹.

Extending the photoresponse spectrum beyond that of silicon (about 1.1 μ m) is vital for modern photodetector technologies for infrared spectrometry, imaging and night-vision applications¹⁶. 2D materials with zero or narrow bandgap, such as graphene, BP and Weyl semimetals, are promising candidates for heterostructures for sensitive infrared light detection¹⁴. For instance, an InSe/BP vdW heterostructure can support impact ionization, yielding avalanche photodetectors with a carrier gain²⁵² of about 10⁴. Besides narrow-bandgap vdW materials, interlayer excitons with infrared absorption can be realized by constructing heterostructures based on two wide-bandgap vdW materials with rationally engineered band alignment²⁵³. For example,

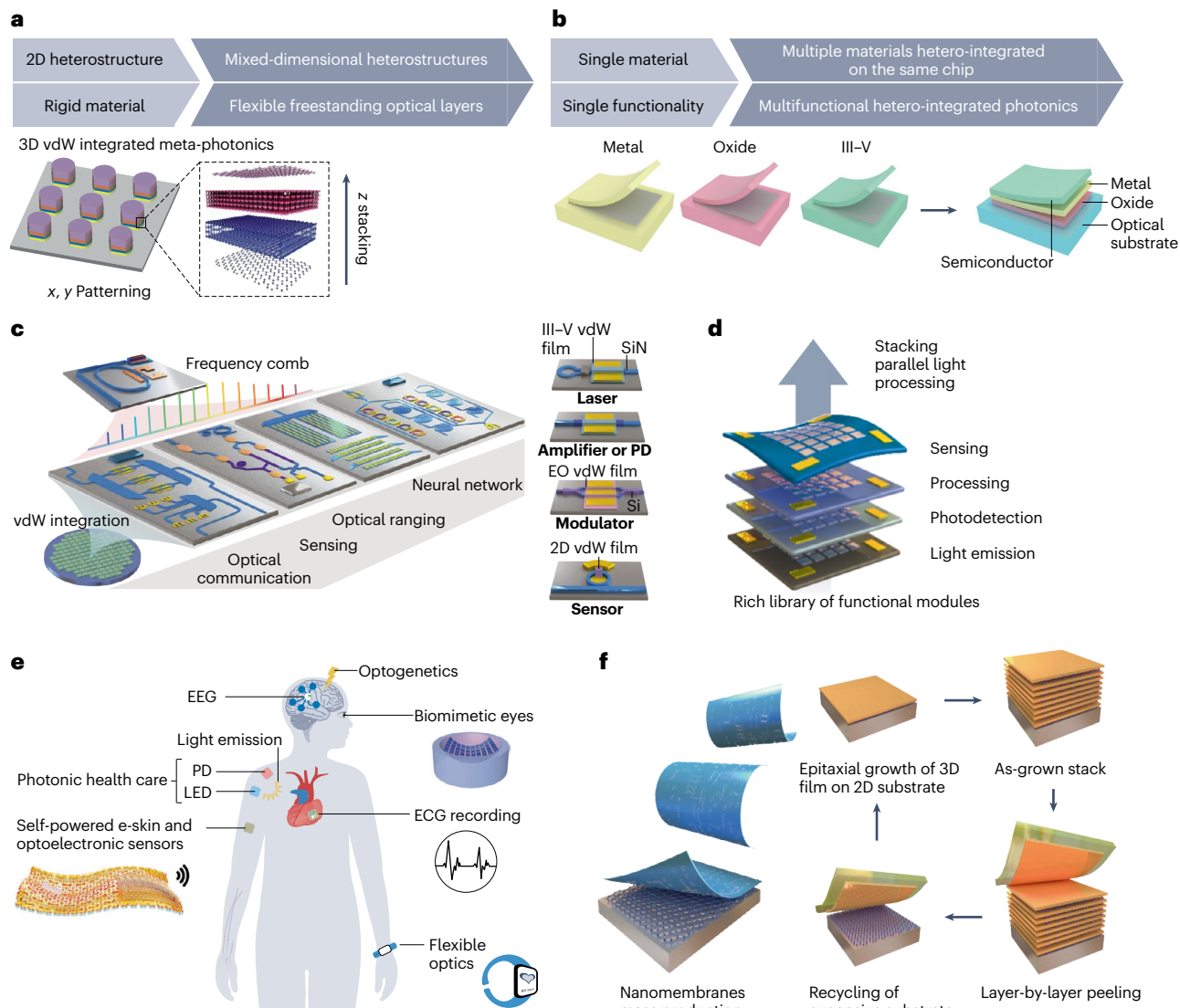


Fig. 7 | Perspectives for freestanding nanomembranes for photonic vdW integration. **a**, The advent of freestanding nanomembranes extends the concept of van der Waals (vdW) heterostructures beyond 2D materials, facilitating vdW meta-photonics^{32,33}. **b**, Photonic vdW integration enables the heterogeneous integration of diverse functional materials⁵. **c**, Advanced hetero-integrated photonic devices based on the transfer and integration of functional vdW films^{28,265}. An electro-optical (EO) frequency comb can drive optical systems with various functionalities, leveraging diverse hetero-integrated photonic devices, such as Si or SiN bus waveguides, Mach–Zehnder waveguides and microrings with integrated III–V,

EO, magneto-optical and 2D films. **d**, 3D photonic integration based on the vertical stacking and coupling of functional layers^{35,36}. **e**, Wearable, implantable and bio-compatible optoelectronic applications enabled by 2D and 3D freestanding films³⁷, such as a biomimetic eye based on Si films and a self-powered e-skin based on GaN films. **f**, The possibility to recycle expensive wafers for nanomembrane production reduces cost⁴¹. ECG, electrocardiogram; EEG, electroencephalograph; LED, light-emitting diode; PD, photodetector. Panel **e** (e-skin) modified from ref. 48. © The Authors, some rights reserved; exclusive licensee AAAS. Panel **e** (biomimetic eye) adapted from ref. 192, Springer Nature Limited.

tightly bound interlayer excitons with a high oscillator strength are observed in WS_2/HfS_2 vdW heterostructures with enhanced absorption compared with the parent materials (WS_2 and HfS_2), which is promising for sensitive infrared detection (Fig. 6g).

vdW integration of 2D–3D heterostructures can result in appealing optoelectronic properties. First, 3D nanomembranes possess much longer optical thickness for light absorption than 2D materials²⁵⁴. Second, 3D materials provide electrical contact for trapping or conducting photogenerated carriers²⁵⁵. For instance, long-lived trapped carriers

generate a photogating effect and result in a high photoconductive gain. This photogating can be enhanced by constructing vdW heterostructures comprising graphene and periodic Si nanostructures with enhanced surface electric field for charge trapping²⁵⁶. Third, emergent photoelectric phenomena can be observed at the 2D–3D interface²⁰. For instance, photoelectric conversion and long-time photocarrier storage have been realized in a p–n junction comprising a WS_2 layer and the quasi-2D electron gas hosted in $SrTiO_3$ (ref. 257) (Fig. 6h). In this heterostructure, the ratio between the current in the fully photo-charged

state and that in the empty photocarrier state is 10^9 , corresponding to an external quantum efficiency of over 93% for optical charging²⁵⁷. This photo-charging and storage can be attributed to a chargeable photo-conductivity effect sustained by the intrinsic space-charge region at the $\text{WS}_2/\text{SrTiO}_3$ boundary.

Metasurfaces can also be integrated with vdW heterostructures for photodetection, resulting in improved sensitivity via enhanced light–matter interactions and responsivity to multiple light attributes such as polarization, direction and orbital angular momentum. When a metasurface with broken inversion symmetry is used, photoexcited hot carriers in graphene can gain an in-plane momentum to generate a shift current, supporting a non-zero photovoltage dependent on linear light polarization²⁵⁸. Mid-infrared photodetectors with linear-polarization response can thus be operated at zero voltage and room temperature. The breaking of in-plane inversion symmetry and the generation of directional hot-carrier transport can be also realized by designing a metasurface with tapered nanoantennas¹⁵⁵. Photodetectors that cannot be realized with natural materials can be fabricated with metasurfaces integrated with vdW materials. For example, a circular-polarization detector, which could be used in chiral sensing owing to its response to the Stokes parameter, was fabricated using an achiral metasurface with preserved mirror symmetry, which induces identical absorption for left and right circularly polarized light, but vectorial photocurrents with opposite signs²⁵⁹ (Fig. 6i).

Outlook

In summary, freestanding nanomembranes offer a promising avenue to heterogeneously integrate dissimilar material systems with disparate crystal structures. Unlike conventional heteroepitaxial approaches, which have fundamental constraints on lattice matching and processing similarity, photonic vdW integration enables the combination of diverse 2D and 3D crystalline thin films with prefabricated photonic structures. The abundance of available optical functionalities and flexibility of layer integration also provide the opportunity to investigate interfacial nanophotonic phenomena in artificial heterostructures and enable new optoelectronic applications.

Despite the exciting progress made on photonic vdW integration of freestanding nanomembranes, several practical challenges remain to be solved to enable fully viable technologies^{19,260}. For 2D vdW films, the large-scale preparation and transfer of high-quality 2D films to non-planar optical structures with clean interfaces and few defects require further optimization to enable the commercialization of 2D photonic devices. The confined growth of 2D monolayers and bilayer heterostructures at predefined locations is promising in this regard^{47,135}. For 3D vdW films, techniques for efficient exfoliation, layer bonding and well controlled nanomembrane transfer^{20,22} are needed for practical photonic vdW integration (Supplementary Information section 5).

In terms of opportunities, the advent of 3D freestanding nanomembranes extends the scope of vdW heterostructures beyond 2D materials¹¹. In conventional flat optics, controlling photon propagation along the vertical direction is challenging^{32,261,262}. vdW heterostructures enable the on-demand vertical stacking of materials with different optical properties to explore nanophotonic polaritons, while the in-plane structures can be controlled by nanofabrication (Fig. 7a). In vdW heterostructures with high index contrast, the out-of-plane symmetry can be broken with easy-to-fabricate straight-sidewall nanostructures. The layer-by-layer coupling of vdW films also enables optical superlattices for the 3D control of photon propagation, allowing

the integration of multiple physical properties in meta-devices^{33,143}. For instance, the vdW integration of EO and MO materials with emitters can produce ultracompact functional light-emitting devices with tuneable polarization and light propagation direction.

Given that a single material can scarcely meet the growing needs of advanced functions and versatilities, photonic integrated circuits and systems-on-chip are gaining in importance. vdW integration enables the co-integration of multiple materials with different optoelectronic responses in the same photonic chip^{7,8} (Fig. 7b), either via vertical stacking or via lateral stitching through spatially aligned microtransfer^{20,23}. Given the ample choice of 2D and 3D functional freestanding nanomembranes, the synergistic integration of III–V semiconductors, EO and MO materials and metal films can potentially revolutionize hetero-integrated photonics^{16–18,28} by providing optical devices with enhanced performance and unprecedented multifunctionality (Fig. 7c).

Furthermore, the surging demand for data-intensive computations and multifunctional optoelectronic systems can hardly be satisfied by discrete improvements of individual optical elements³⁵. Vertically integrated 2D and 3D freestanding films could be used to this end³⁶ (Fig. 7d). Advanced layer transfer and nanofabrication techniques permit stackable 3D architectures with very high integration density, efficient interlayer communication and parallel optical information-processing capabilities for optical interconnects and artificial intelligence^{47,263}. A new platform to explore the coupling between light and a variety of physical fields can also be envisioned^{8,20}.

Finally, ultrathin freestanding nanomembranes hold promise for flexible optoelectronic applications, such as wearable photonic devices, implantable biosensors and photo-diagnostic applications^{37,192} (Fig. 7e). The universal film exfoliation process in vdW and remote epitaxy also enables the recycling of the expensive wafers used as substrate, such as GaAs, GaN and InP, which can be reused to grow new nanomembranes⁴¹ (Fig. 7f). The possibility of using a universal platform for manufacturing single-crystalline optical nanomembranes in a low-cost, fast and high-throughput manner lays a promising foundation for the commercialization of non-Si photonics^{22,43,65,264}.

Published online: 21 April 2023

References

- Zhang, Q. et al. Interface nano-optics with van der Waals polaritons. *Nature* **597**, 187–195 (2021).
 - Kaur, P. et al. Hybrid and heterogeneous photonic integration. *APL Photon.* **6**, 061102 (2021).
 - Marpaung, D., Yao, J. & Capmany, J. Integrated microwave photonics. *Nat. Photon.* **13**, 80–90 (2019).
 - Bogaerts, W. et al. Programmable photonic circuits. *Nature* **586**, 207–216 (2020).
 - Kim, I. et al. Nanophotonics for light detection and ranging technology. *Nat. Nanotechnol.* **16**, 508–524 (2021).
 - Altug, H., Oh, S.-H., Maier, S. A. & Homola, J. Advances and applications of nanophotonic biosensors. *Nat. Nanotechnol.* **17**, 5–16 (2022).
 - Elshaari, A. W., Pernice, W., Srinivasan, K., Benson, O. & Zwiller, V. Hybrid integrated quantum photonic circuits. *Nat. Photon.* **14**, 285–298 (2020).
 - Kum, H. S. et al. Heterogeneous integration of single-crystalline complex-oxide membranes. *Nature* **578**, 75–81 (2020).
- This paper reports the fabrication of novel artificial heterostructures by stacking freestanding 3D complex oxide nanomembranes.**
- Castellanos-Gomez, A. et al. Van der Waals heterostructures. *Nat. Rev. Methods Primers* **2**, 58 (2022).
 - Matthews, J. & Blakeslee, A. Defects in epitaxial multilayers: I. Misfit dislocations. *J. Cryst. Growth* **27**, 118–125 (1974).
 - Liu, Y., Huang, Y. & Duan, X. Van der Waals integration before and beyond two-dimensional materials. *Nature* **567**, 323–333 (2019).
- This review outlines the progress of vdW integration beyond 2D materials for electronic applications.**
- Liu, Y. et al. Van der Waals heterostructures and devices. *Nat. Rev. Mater.* **1**, 16042 (2016).

13. Geim, A. K. & Grigorieva, I. V. Van der Waals heterostructures. *Nature* **499**, 419–425 (2013).
14. Novoselov, K., Mishchenko, A., Carvalho, A. & Castro Neto, A. H. 2D materials and van der Waals heterostructures. *Science* **353**, aac9439 (2016).
15. Wilson, N. P., Yao, W., Shan, J. & Xu, X. Excitons and emergent quantum phenomena in stacked 2D semiconductors. *Nature* **599**, 383–392 (2021).
16. Liu, C. et al. Silicon/2D-material photodetectors: from near-infrared to mid-infrared. *Light Sci. Appl.* **10**, 123 (2021).
17. Regan, E. C. et al. Emerging excite physics in transition metal dichalcogenide heterobilayers. *Nat. Rev. Mater.* **7**, 778–795 (2022).
18. Turunen, M. et al. Quantum photonics with layered 2D materials. *Nat. Rev. Phys.* **4**, 219–236 (2022).
19. Kong, W. et al. Path towards graphene commercialization from lab to market. *Nat. Nanotechnol.* **14**, 927–938 (2019).
20. Bae, S.-H. et al. Integration of bulk materials with two-dimensional materials for physical coupling and applications. *Nat. Mater.* **18**, 550–560 (2019).
- This review describes the advent of 3D freestanding nanomembranes and their electronic and optoelectronic applications with 2D materials.**
21. Carlson, A., Bowen, A. M., Huang, Y., Nuzzo, R. G. & Rogers, J. A. Transfer printing techniques for materials assembly and micro/nanodevice fabrication. *Adv. Mater.* **24**, 5284–5318 (2012).
22. Kum, H. et al. Epitaxial growth and layer-transfer techniques for heterogeneous integration of materials for electronic and photonic devices. *Nat. Electron.* **2**, 439–450 (2019).
- A comprehensive review on advanced thin-film epitaxy, layer lift-off and nanomembrane transfer techniques towards applications.**
23. Kim, H. et al. Remote epitaxy. *Nat. Rev. Methods Primers* **2**, 40 (2022).
24. Yoon, J. et al. Heterogeneously integrated optoelectronic devices enabled by micro-transfer printing. *Adv. Opt. Mater.* **3**, 1313–1335 (2015).
25. Ning, C.-Z., Dou, L. & Yang, P. Bandgap engineering in semiconductor alloy nanomaterials with widely tunable compositions. *Nat. Rev. Mater.* **2**, 17070 (2017).
26. Qu, G. et al. Property–activity relationship of black phosphorus at the nano–bio interface: from molecules to organisms. *Chem. Rev.* **120**, 2288–2346 (2020).
27. Castellanos-Gomez, A. Why all the fuss about 2D semiconductors? *Nat. Photon.* **10**, 202–204 (2016).
28. Tran, M. et al. Extending the spectrum of fully integrated photonics. *Nature* **610**, 54–60 (2022).
- This paper demonstrates essential integrated photonic circuit building blocks by hetero-integrating III–V materials with SiN waveguides.**
29. Liang, D. & Bowers, J. E. Recent progress in heterogeneous III–V-on-silicon photonic integration. *Light Adv. Manuf.* **2**, 59–83 (2021).
30. Wang, C. et al. Integrated lithium niobate electro-optic modulators operating at CMOS-compatible voltages. *Nature* **562**, 101–104 (2018).
31. Sun, D. et al. Microstructure and domain engineering of lithium niobate crystal films for integrated photonic applications. *Light Sci. Appl.* **9**, 197 (2020).
32. Dai, Z. et al. Artificial metaphotonics born naturally in two dimensions. *Chem. Rev.* **120**, 6197–6246 (2020).
33. Lin, H. et al. Engineering van der Waals materials for advanced metaphotonics. *Chem. Rev.* **122**, 15204–15355 (2022).
34. Najafi, F. et al. On-chip detection of non-classical light by scalable integration of single-photon detectors. *Nat. Commun.* **6**, 5873 (2015).
35. Shulaker, M. M. et al. Three-dimensional integration of nanotechnologies for computing and data storage on a single chip. *Nature* **547**, 74–78 (2017).
36. Choi, C. et al. Reconfigurable heterogeneous integration using stackable chips with embedded artificial intelligence. *Nat. Electron.* **5**, 386–393 (2022).
- This paper reports a hetero-integrated optoelectronic system by vertically stacking different freestanding nanomembranes with embedded memristors.**
37. Lee, G.-H. et al. Multifunctional materials for implantable and wearable photonic healthcare devices. *Nat. Rev. Mater.* **5**, 149–165 (2020).
38. Geiger, S. et al. Flexible and stretchable photonics: the next stretch of opportunities. *ACS Photon.* **7**, 2618–2635 (2020).
39. Rickman, A. The commercialization of silicon photonics. *Nat. Photon.* **8**, 579–582 (2014).
40. Ren, F. et al. Van der Waals epitaxy of nearly single-crystalline nitride films on amorphous graphene-glass wafer. *Sci. Adv.* **7**, eabf5011 (2021).
41. Kim, H. et al. High-throughput manufacturing of epitaxial membranes from a single wafer by 2D materials-based layer transfer. *Nat. Nanotechnol.* <https://doi.org/10.1038/s41565-023-01340-3> (2023).
42. Kim, H. et al. Graphene nanopattern as a universal epitaxy platform for single-crystal membrane production and defect reduction. *Nat. Nanotechnol.* **17**, 1054–1059 (2022).
43. Kim, Y. et al. Remote epitaxy through graphene enables two-dimensional material-based layer transfer. *Nature* **544**, 340–343 (2017).
44. Yang, A. J. et al. Van der Waals integration of high- κ perovskite oxides and two-dimensional semiconductors. *Nat. Electron.* **5**, 233–240 (2022).
45. Neto, A. C., Guinea, F., Peres, N. M., Novoselov, K. S. & Geim, A. K. The electronic properties of graphene. *Rev. Mod. Phys.* **81**, 109 (2009).
46. Manzeli, S., Ovchinnikov, D., Pasquier, D., Yazyev, O. V. & Kis, A. 2D transition metal dichalcogenides. *Nat. Rev. Mater.* **2**, 17033 (2017).
47. Akinwande, D. et al. Graphene and two-dimensional materials for silicon technology. *Nature* **573**, 507–518 (2019).
48. Kim, Y. et al. Chip-less wireless electronic skins by remote epitaxial freestanding compound semiconductors. *Science* **377**, 859–864 (2022).
49. Sun, Z., Martinez, A. & Wang, F. Optical modulators with 2D layered materials. *Nat. Photon.* **10**, 227–238 (2016).
50. Aspar, B. et al. The generic nature of the Smart-Cut® process for thin film transfer. *J. Electron. Mater.* **30**, 834–840 (2001).
51. Tanaka, A. et al. Smart-cut-like laser slicing of GaN substrate using its own nitrogen. *Sci. Rep.* **11**, 17949 (2021).
52. Bedell, S. W. et al. Layer transfer by controlled spalling. *J. Phys. D* **46**, 152002 (2013).
53. Bedell, S. W. et al. Kerf-less removal of Si, Ge, and III–V layers by controlled spalling to enable low-cost PV technologies. *IEEE J. Photovolt.* **2**, 141–147 (2012).
54. Park, H. et al. Layer-resolved release of epitaxial layers in III–V heterostructure via a buffer-free mechanical separation technique. *Sci. Adv.* **8**, eabl6406 (2022).
55. Wang, Q. H., Kalantar-Zadeh, K., Kis, A., Coleman, J. N. & Strano, M. S. Electronics and optoelectronics of two-dimensional transition metal dichalcogenides. *Nat. Nanotechnol.* **7**, 699–712 (2012).
56. Yu, S., Wu, X., Wang, Y., Guo, X. & Tong, L. 2D materials for optical modulation: challenges and opportunities. *Adv. Mater.* **29**, 1606128 (2017).
57. Guo, Q. et al. Ultrathin quantum light source with van der Waals NbOCl₂ crystal. *Nature* **613**, 53–59 (2023).
- To our knowledge, this study reports for the first time spontaneous parametric downconversion from quantum sources based on 2D layered materials with vanishing interlayer electronic coupling.**
58. Abdelwahab, I. et al. Giant second-harmonic generation in ferroelectric NbO₂. *Nat. Photon.* **16**, 644–650 (2022).
59. Ma, W. et al. In-plane anisotropic and ultra-low-loss polaritons in a natural van der Waals crystal. *Nature* **562**, 557–562 (2018).
- This study reports the first observation of in-plane hyperbolic phonon polaritons in α -MoO₃.**
60. Hu, G. et al. Topological polaritons and photonic magic angles in twisted α -MoO₃ bilayers. *Nature* **582**, 209–213 (2020).
- This study reports twisted α -MoO₃ bilayers with topological transitions of polariton dispersion.**
61. Zhang, Q. et al. Unidirectionally excited phonon polaritons in high-symmetry orthorhombic crystals. *Sci. Adv.* **8**, eabn9774 (2022).
62. Huang, B. et al. Layer-dependent ferromagnetism in a van der Waals crystal down to the monolayer limit. *Nature* **546**, 270–273 (2017).
63. Gong, C. et al. Discovery of intrinsic ferromagnetism in two-dimensional van der Waals crystals. *Nature* **546**, 265–269 (2017).
64. Zhang, D., Schoenherr, P., Sharma, P. & Seidel, J. Ferroelectric order in van der Waals layered materials. *Nat. Rev. Mater.* **8**, 25–40 (2023).
65. Kong, W. et al. Polarity governs atomic interaction through two-dimensional materials. *Nat. Mater.* **17**, 999–1004 (2018).
66. Chu, Y.-H. Van der Waals oxide heteroepitaxy. *npj Quantum Mater.* **2**, 67 (2017).
67. Zakharian, A. R., Moloney, J. V. & Mansuripur, M. Surface plasmon polaritons on metallic surfaces. *Opt. Express* **15**, 183–197 (2007).
68. Wu, Y. et al. Manipulating polaritons at the extreme scale in van der Waals materials. *Nat. Rev. Phys.* **4**, 578–594 (2022).
69. Hu, Y. et al. On-chip electro-optic frequency shifters and beam splitters. *Nature* **599**, 587–593 (2021).
70. Zhu, D. et al. Integrated photonics on thin-film lithium niobate. *Adv. Opt. Photon.* **13**, 242–352 (2021).
- A comprehensive review of LiNbO₃ thin-films-based integrated photonics.**
71. Wang, C., Zhang, M., Stern, B., Lipson, M. & Lončar, M. Nanophotonic lithium niobate electro-optic modulators. *Opt. Express* **26**, 1547–1555 (2018).
72. He, M. et al. High-performance hybrid silicon and lithium niobate Mach–Zehnder modulators for 100 Gbit s⁻¹ and beyond. *Nat. Photon.* **13**, 359–364 (2019).
73. Li, M. et al. Lithium niobate photonic-crystal electro-optic modulator. *Nat. Commun.* **11**, 4123 (2020).
74. Guarino, A., Poberaj, G., Rezzonico, D., Degl’Innocenti, R. & Günter, P. Electro-optically tunable microring resonators in lithium niobate. *Nat. Photon.* **1**, 407–410 (2007).
75. Zhang, M. et al. Broadband electro-optic frequency comb generation in a lithium niobate microring resonator. *Nature* **568**, 373–377 (2019).
76. Rueda, A., Sedlmeir, F., Kumari, M., Leuchs, G. & Schwefel, H. G. Resonant electro-optic frequency comb. *Nature* **568**, 378–381 (2019).
77. Pohl, D. et al. An integrated broadband spectrometer on thin-film lithium niobate. *Nat. Photon.* **14**, 24–29 (2020).
78. Arrangoiz-Arriola, P. et al. Resolving the energy levels of a nanomechanical oscillator. *Nature* **571**, 537–540 (2019).
79. Dong, G. et al. Super-elastic ferroelectric single-crystal membrane with continuous electric dipole rotation. *Science* **366**, 475–479 (2019).
80. Karvounis, A., Timpu, F., Vogler-Neuling, V. V., Savo, R. & Grange, R. BaTiO₃: barium titanate nanostructures and thin films for photonics. *Adv. Opt. Mater.* **8**, 2070094 (2020).
81. Xiong, C. et al. Active silicon integrated nanophotonics: ferroelectric BaTiO₃ devices. *Nano Lett.* **14**, 1419–1425 (2014).
82. Abel, S. et al. Large Pockels effect in micro- and nanostructured barium titanate integrated on silicon. *Nat. Mater.* **18**, 42–47 (2019).
83. Geler-Kremer, J. et al. A ferroelectric multilevel non-volatile photonic phase shifter. *Nat. Photon.* **16**, 491–497 (2022).

84. Bi, L. et al. On-chip optical isolation in monolithically integrated non-reciprocal optical resonators. *Nat. Photon.* **5**, 758–762 (2011).
 85. Pintus, P. et al. An integrated magneto-optic modulator for cryogenic applications. *Nat. Electron.* **5**, 604–610 (2022).
 86. Merbouche, H. et al. Giant nonlinear self-phase modulation of large-amplitude spin waves in microscopic YIG waveguides. *Sci. Rep.* **12**, 7246 (2022).
 87. Wang, F. et al. Gate-variable optical transitions in graphene. *Science* **320**, 206–209 (2008).
 88. Woessner, A. et al. Highly confined low-loss plasmons in graphene–boron nitride heterostructures. *Nat. Mater.* **14**, 421–425 (2015).
 89. Ju, L. et al. Graphene plasmonics for tunable terahertz metamaterials. *Nat. Nanotechnol.* **6**, 630–634 (2011).
 90. Low, T. et al. Polaritons in layered two-dimensional materials. *Nat. Mater.* **16**, 182–194 (2017).
 91. Koppens, F. et al. Photodetectors based on graphene, other two-dimensional materials and hybrid systems. *Nat. Nanotechnol.* **9**, 780–793 (2014).
 92. Mak, K. F., Lee, C., Hone, J., Shan, J. & Heinz, T. F. Atomically thin MoS₂: a new direct-gap semiconductor. *Phys. Rev. Lett.* **105**, 136805 (2010).
 93. Wang, G. et al. Colloquium: Excitons in atomically thin transition metal dichalcogenides. *Rev. Mod. Phys.* **90**, 021001 (2018).
 94. Zeng, H., Dai, J., Yao, W., Xiao, D. & Cui, X. Valley polarization in MoS₂ monolayers by optical pumping. *Nat. Nanotechnol.* **7**, 490–493 (2012).
 95. Schaibley, J. R. et al. Valleytronics in 2D materials. *Nat. Rev. Mater.* **1**, 16055 (2016).
 96. Xia, F., Wang, H., Hwang, J., Neto, A. & Yang, L. Black phosphorus and its isoelectronic materials. *Nat. Rev. Phys.* **1**, 306–317 (2019).
 97. Yuan, H. et al. Polarization-sensitive broadband photodetector using a black phosphorus vertical p–n junction. *Nat. Nanotechnol.* **10**, 707–713 (2015).
 98. Kim, H. et al. Actively variable-spectrum optoelectronics with black phosphorus. *Nature* **596**, 232–237 (2021).
 99. Kim, C.-J. et al. Stacking order dependent second harmonic generation and topological defects in h-BN bilayers. *Nano Lett.* **13**, 5660–5665 (2013).
 100. Yoxall, E. et al. Direct observation of ultraslow hyperbolic polariton propagation with negative phase velocity. *Nat. Photon.* **9**, 674–678 (2015).
 101. Tran, T. T., Bray, K., Ford, M. J., Toth, M. & Aharonovich, I. Quantum emission from hexagonal boron nitride monolayers. *Nat. Nanotechnol.* **11**, 37–41 (2016).
 102. Ricciardulli, A. G., Yang, S., Smet, J. H. & Saliba, M. Emerging perovskite monolayers. *Nat. Mater.* **20**, 1325–1336 (2021).
 103. Leng, K., Fu, W., Liu, Y., Chhowalla, M. & Loh, K. P. From bulk to molecularly thin hybrid perovskites. *Nat. Rev. Mater.* **5**, 482–500 (2020).
 104. Blancon, J.-C., Even, J., Stoumpos, C., Kanatzidis, M. & Mohite, A. D. Semiconductor physics of organic–inorganic 2D halide perovskites. *Nat. Nanotechnol.* **15**, 969–985 (2020).
 105. Su, R. et al. Perovskite semiconductors for room-temperature exciton-polaritronics. *Nat. Mater.* **20**, 1315–1324 (2021).
 106. Yuan, M. et al. Perovskite energy funnels for efficient light-emitting diodes. *Nat. Nanotechnol.* **11**, 872–877 (2016).
 107. Wang, N. et al. Perovskite light-emitting diodes based on solution-processed self-organized multiple quantum wells. *Nat. Photon.* **10**, 699–704 (2016).
 108. Quan, L. N., Garcia de Arquer, F. P., Sabatini, R. P. & Sargent, E. H. Perovskites for light emission. *Adv. Mater.* **30**, 1801996 (2018).
 109. Feng, J. et al. Single-crystalline layered metal-halide perovskite nanowires for ultrasensitive photodetectors. *Nat. Electron.* **1**, 404–410 (2018).
 110. Long, G. et al. Spin control in reduced-dimensional chiral perovskites. *Nat. Photon.* **12**, 528–533 (2018).
 111. Xu, J. et al. Halide perovskites for nonlinear optics. *Adv. Mater.* **32**, 1806736 (2020).
 112. Li, L. et al. Tailored engineering of an unusual (C₄H₉NH₃)₂(CH₃NH₂)₂Pb₃Br₁₀ two-dimensional multilayered perovskite ferroelectric for a high-performance photodetector. *Angew. Chem. Int. Ed.* **129**, 12318–12322 (2017).
 113. Derry, G. N., Kern, M. E. & Worth, E. H. Recommended values of clean metal surface work functions. *J. Vac. Sci. Technol. A* **33**, 060801 (2015).
 114. Wang, Y. et al. Probing photoelectrical transport in lead halide perovskites with van der Waals contacts. *Nat. Nanotechnol.* **15**, 768–775 (2020).
 115. Kong, L. et al. Doping-free complementary WSe₂ circuit via van der Waals metal integration. *Nat. Commun.* **11**, 1866 (2020).
 116. Yoon, J. et al. *Ultrathin Silicon Solar Microcells For Semitransparent, Mechanically Flexible And Microconcentrator Module Designs* (World Scientific/Nature Publishing Group, 2011).
 117. Yoon, J. et al. Flexible concentrator photovoltaics based on microscale silicon solar cells embedded in luminescent waveguides. *Nat. Commun.* **2**, 343 (2011).
 118. Cheng, Y.-B., Pascoe, A., Huang, F. & Peng, Y. Print flexible solar cells. *Nature* **539**, 488–489 (2016).
 119. Zhang, J. et al. III–V-on-Si photonic integrated circuits realized using micro-transfer-printing. *APL Photon.* **4**, 110803 (2019).
 120. Dietrich, C. P., Fiore, A., Thompson, M. G., Kamp, M. & Höfling, S. GaAs integrated quantum photonics: towards compact and multi-functional quantum photonic integrated circuits. *Laser Photon. Rev.* **10**, 870–894 (2016).
 121. Smit, M., Williams, K. & Van Der Tol, J. Past, present, and future of InP-based photonic integration. *APL Photon.* **4**, 050901 (2019).
 122. Hong, X. et al. Ultrafast charge transfer in atomically thin MoS₂/WS₂ heterostructures. *Nat. Nanotechnol.* **9**, 682–686 (2014).
 123. Jin, C. et al. Ultrafast dynamics in van der Waals heterostructures. *Nat. Nanotechnol.* **13**, 994–1003 (2018).
 124. Rivera, P. et al. Observation of long-lived interlayer excitons in monolayer MoSe₂–WSe₂ heterostructures. *Nat. Commun.* **6**, 6242 (2015).
 125. Rivera, P. et al. Valley-polarized exciton dynamics in a 2D semiconductor heterostructure. *Science* **351**, 688–691 (2016).
 126. Ciarrocchi, A. et al. Polarization switching and electrical control of interlayer excitons in two-dimensional van der Waals heterostructures. *Nat. Photon.* **13**, 131–136 (2019).
 127. Jauregui, L. A. et al. Electrical control of interlayer exciton dynamics in atomically thin heterostructures. *Science* **366**, 870–875 (2019).
 128. Wu, F., Lovorn, T., Tutuc, E. & MacDonald, A. H. Hubbard model physics in transition metal dichalcogenide moiré bands. *Phys. Rev. Lett.* **121**, 026402 (2018).
 129. Huang, D., Choi, J., Shih, C.-K. & Li, X. Excitons in semiconductor moiré superlattices. *Nat. Nanotechnol.* **17**, 227–238 (2022).
 130. Cao, Y. et al. Unconventional superconductivity in magic-angle graphene superlattices. *Nature* **556**, 43–50 (2018).
 131. Cao, Y. et al. Correlated insulator behaviour at half-filling in magic-angle graphene superlattices. *Nature* **556**, 80–84 (2018).
 132. Regan, E. C. et al. Mott and generalized Wigner crystal states in WSe₂/WS₂ moiré superlattices. *Nature* **579**, 359–363 (2020).
 133. Novoselov, K. A roadmap for graphene. *Nature* **490**, 192–200 (2012).
 134. Shim, J. et al. Controlled crack propagation for atomic precision handling of wafer-scale two-dimensional materials. *Science* **362**, 665–670 (2018).
 135. Kim, K. S. et al. Non-epitaxial single-crystal 2D material growth by geometrical confinement. *Nature* **614**, 88–94 (2023).
- This study reports high-quality wafer-scale 2D TMD monolayers and bilayer heterostructures on industrial wafers with predefined growth pockets.**
136. Lee, K., Zimmerman, J. D., Xiao, X., Sun, K. & Forrest, S. R. Reuse of GaAs substrates for epitaxial lift-off by employing protection layers. *J. Appl. Phys.* **111**, 033527 (2012).
 137. Yablonoitch, E., Gmitter, T., Harbison, J. & Bhat, R. Extreme selectivity in the lift-off of epitaxial GaAs films. *Appl. Phys. Lett.* **51**, 2222–2224 (1987).
 138. Wong, W. et al. Fabrication of thin-film InGaN light-emitting diode membranes by laser lift-off. *Appl. Phys. Lett.* **75**, 1360–1362 (1999).
 139. Wong, W., Sands, T. & Cheung, N. Damage-free separation of GaN thin films from sapphire substrates. *Appl. Phys. Lett.* **72**, 599–601 (1998).
 140. Kim, J. et al. Principle of direct van der Waals epitaxy of single-crystalline films on epitaxial graphene. *Nat. Commun.* **5**, 4836 (2014).
 141. Meng, Y. et al. Waveguide engineering of graphene optoelectronics — modulators and polarizers. *IEEE Photon. J.* **10**, 6600217 (2018).
 142. Shao, L. et al. Non-reciprocal transmission of microwave acoustic waves in nonlinear parity–time symmetric resonators. *Nat. Electron.* **3**, 267–272 (2020).
 143. Meng, Y. et al. Optical meta-waveguides for integrated photonics and beyond. *Light Sci. Appl.* **10**, 235 (2021).
 144. Zhang, L. et al. High-performance quasi-2D perovskite light-emitting diodes: from materials to devices. *Light Sci. Appl.* **10**, 61 (2021).
 145. Jiang, T. et al. Gate-tunable third-order nonlinear optical response of massless Dirac fermions in graphene. *Nat. Photon.* **12**, 430–436 (2018).
 146. Grigorenko, A. N., Polini, M. & Novoselov, K. Graphene plasmonics. *Nat. Photon.* **6**, 749–758 (2012).
 147. Liu, M. et al. A graphene-based broadband optical modulator. *Nature* **474**, 64–67 (2011).
 148. Kim, K., Choi, J.-Y., Kim, T., Cho, S.-H. & Chung, H.-J. A role for graphene in silicon-based semiconductor devices. *Nature* **479**, 338–344 (2011).
 149. Lin, H. et al. Chalcogenide glass-on-graphene photonics. *Nat. Photon.* **11**, 798–805 (2017).
 150. Gan, S. et al. A highly efficient thermo-optic microring modulator assisted by graphene. *Nanoscale* **7**, 20249–20255 (2015).
 151. Sorianello, V. et al. Graphene–silicon phase modulators with gigahertz bandwidth. *Nat. Photon.* **12**, 40–44 (2018).
 152. Woessner, A. et al. Electrical 2π phase control of infrared light in a 350-nm footprint using graphene plasmons. *Nat. Photon.* **11**, 421–424 (2017).
 153. Ono, M. et al. Ultrafast and energy-efficient all-optical switching with graphene-loaded deep-subwavelength plasmonic waveguides. *Nat. Photon.* **14**, 37–43 (2020).
 154. Xu, R. et al. Strain-induced room-temperature ferroelectricity in SrTiO₃ membranes. *Nat. Commun.* **11**, 3141 (2020).
 155. Wei, J., Xu, C., Dong, B., Qiu, C.-W. & Lee, C. Mid-infrared semimetal polarization detectors with configurable polarity transition. *Nat. Photon.* **15**, 614–621 (2021).
 156. Xiong, L. et al. Photonic crystal for graphene plasmons. *Nat. Commun.* **10**, 4780 (2019).
 157. Buscema, M. et al. Photocurrent generation with two-dimensional van der Waals semiconductors. *Chem. Soc. Rev.* **44**, 3691–3718 (2015).
 158. Chen, Y. et al. Unipolar barrier photodetectors based on van der Waals heterostructures. *Nat. Electron.* **4**, 357–363 (2021).
 159. Alonso Calafell, I. et al. Giant enhancement of third-harmonic generation in graphene–metal heterostructures. *Nat. Nanotechnol.* **16**, 318–324 (2021).
 160. Yao, B. et al. Gate-tunable frequency combs in graphene–nitride microresonators. *Nature* **558**, 410–414 (2018).
 161. Bunch, J. S. et al. Electromechanical resonators from graphene sheets. *Science* **315**, 490–493 (2007).
 162. Nikitin, A. et al. Real-space mapping of tailored sheet and edge plasmons in graphene nanoresonators. *Nat. Photon.* **10**, 239–243 (2016).

163. Vakil, A. & Engheta, N. Transformation optics using graphene. *Science* **332**, 1291–1294 (2011).
164. Jiang, T., Kravtsov, V., Tokman, M., Belyanin, A. & Raschke, M. B. Ultrafast coherent nonlinear nanooptics and nanoimaging of graphene. *Nat. Nanotechnol.* **14**, 838–843 (2019).
165. Fei, Z. et al. Gate-tuning of graphene plasmons revealed by infrared nano-imaging. *Nature* **487**, 82–85 (2012).
166. Young, S. M. & Kane, C. Dirac semimetals in two dimensions. *Phys. Rev. Lett.* **115**, 126803 (2015).
167. Chaves, A. et al. Bandgap engineering of two-dimensional semiconductor materials. *npj 2D Mater. Appl.* **4**, 29 (2020).
168. Du, W. et al. Nanolasers based on 2D materials. *Laser Photon. Rev.* **14**, 2000271 (2020).
169. Yuan, S., Naveh, D., Watanabe, K., Taniguchi, T. & Xia, F. A wavelength-scale black phosphorus spectrometer. *Nat. Photon.* **15**, 601–607 (2021).
170. Shen, W. et al. Wavelength tunable polarizer based on layered black phosphorus on Si/SiO₂ substrate. *Opt. Lett.* **43**, 1255–1258 (2018).
171. Whitney, W. S. et al. Field effect optoelectronic modulation of quantum-confined carriers in black phosphorus. *Nano Lett.* **17**, 78–84 (2017).
172. van de Groep, J. et al. Exciton resonance tuning of an atomically thin lens. *Nat. Photon.* **14**, 426–430 (2020).
173. Yang, S. et al. CMOS-compatible WS₂-based all-optical modulator. *ACS Photon.* **5**, 342–346 (2018).
174. Knopf, H. et al. Integration of atomically thin layers of transition metal dichalcogenides into high-Q, monolithic Bragg-cavities: an experimental platform for the enhancement of the optical interaction in 2D-materials. *Opt. Mater. Express* **9**, 598–610 (2019).
175. Trovatello, C. et al. Optical parametric amplification by monolayer transition metal dichalcogenides. *Nat. Photon.* **15**, 6–10 (2021).
176. Li, Y. et al. Room-temperature continuous-wave lasing from monolayer molybdenum ditelluride integrated with a silicon nanobeam cavity. *Nat. Nanotechnol.* **12**, 987–992 (2017).
177. Peyskens, F., Chakraborty, C., Muneeb, M., Van Thourhout, D. & Englund, D. Integration of single photon emitters in 2D layered materials with a silicon nitride photonic chip. *Nat. Commun.* **10**, 4435 (2019).
178. Caldwell, J. D. et al. Photonics with hexagonal boron nitride. *Nat. Rev. Mater.* **4**, 552–567 (2019).
179. Liu, G. et al. Graphene-assisted metal transfer printing for wafer-scale integration of metal electrodes and two-dimensional materials. *Nat. Electron.* **5**, 275–280 (2022).
180. Li, P. et al. Infrared hyperbolic metasurface based on nanostructured van der Waals materials. *Science* **359**, 892–896 (2018).
181. Bourrellier, R. et al. Bright UV single photon emission at point defects in h-BN. *Nano Lett.* **16**, 4317–4321 (2016).
182. Li, Y. et al. Probing symmetry properties of few-layer MoS₂ and h-BN by optical second-harmonic generation. *Nano Lett.* **13**, 3329–3333 (2013).
183. Shahrjerdi, D. & Bedell, S. W. Extremely flexible nanoscale ultrathin body silicon integrated circuits on plastic. *Nano Lett.* **13**, 315–320 (2013).
184. Cheng, C.-W. et al. Epitaxial lift-off process for gallium arsenide substrate reuse and flexible electronics. *Nat. Commun.* **4**, 1577 (2013).
185. Lee, Y., Yang, I., Tan, H. H., Jagadish, C. & Karuturi, S. K. Monocrystalline InP thin films with tunable surface morphology and energy band gap. *ACS Appl. Mater. Interf.* **12**, 36380–36388 (2020).
186. Khandelwal, A. et al. Self-rolled-up aluminum nitride-based 3D architectures enabled by record-high differential stress. *ACS Appl. Mater. Interf.* **14**, 29014–29024 (2022).
187. Poberaj, G., Hu, H., Sohler, W. & Guenter, P. Lithium niobate on insulator (LNOI) for micro-photonics devices. *Laser Photon. Rev.* **6**, 488–503 (2012).
188. Dai, L. et al. Highly heterogeneous epitaxy of flexoelectric BaTiO₃- δ membrane on Ge. *Nat. Commun.* **13**, 2990 (2022).
189. Boroviks, S. et al. Extremely confined gap plasmon modes: when nonlocality matters. *Nat. Commun.* **13**, 3105 (2022).
190. Munkhbat, B., Canales, A., K uc ukb z, B., Baranov, D. G. & Shegai, T. O. Tunable self-assembled Casimir microcavities and polaritons. *Nature* **597**, 214–219 (2021).
191. Sarkar, A., Lee, Y. & Ahn, J.-H. Si nanomembranes: material properties and applications. *Nano Res.* **14**, 3010–3032 (2021).
192. Ko, H. C. et al. A hemispherical electronic eye camera based on compressible silicon optoelectronics. *Nature* **454**, 748–753 (2008).
193. Zhang, K. et al. Origami silicon optoelectronics for hemispherical electronic eye systems. *Nat. Commun.* **8**, 1782 (2017).
194. Sim, K. et al. Three-dimensional curvy electronics created using conformal additive stamp printing. *Nat. Electron.* **2**, 471–479 (2019).
195. Aharonovich, I., Greentree, A. D. & Prawer, S. Diamond photonics. *Nat. Photon.* **5**, 397–405 (2011).
196. Guo, X. et al. Tunable and transferable diamond membranes for integrated quantum technologies. *Nano Lett.* **21**, 10392–10399 (2021).
197. Kreuzer, C., Riedrich-M oller, J., Neu, E. & Becher, C. Design of photonic crystal microcavities in diamond films. *Opt. Express* **16**, 1632–1644 (2008).
198. Castelletto, S., Rosa, L., Blackledge, J., Al Abri, M. Z. & Boretti, A. Advances in diamond nanofabrication for ultrasensitive devices. *Microsyst. Nanoeng.* **3**, 17061 (2017).
199. Wan, N. H. et al. Large-scale integration of artificial atoms in hybrid photonic circuits. *Nature* **583**, 226–231 (2020).
- This study reports the high-yield hetero-integration of diamond nanomembranes with quantum photonic integrated circuits.**
200. Xia, Z. et al. Single-crystalline germanium nanomembrane photodetectors on foreign nanocavities. *Sci. Adv.* **3**, e1602783 (2017).
201. Nam, D. et al. Strained germanium thin film membrane on silicon substrate for optoelectronics. *Opt. Express* **19**, 25866–25872 (2011).
202. Liu, S., Shah, D. S. & Kramer-Bottiglio, R. Highly stretchable multilayer electronic circuits using biphasic gallium–indium. *Nat. Mater.* **20**, 851–858 (2021).
203. Nam, D. et al. Demonstration of electroluminescence from strained Ge membrane LED. in *2012 International Silicon-Germanium Technology and Device Meeting (ISTDM)* 98 (IEEE, 2012).
204. Sheng, X. et al. Transfer printing of fully formed thin-film microscale GaAs lasers on silicon with a thermally conductive interface material. *Laser Photon. Rev.* **9**, L17–L22 (2015).
205. Justice, J. et al. Wafer-scale integration of group III–V lasers on silicon using transfer printing of epitaxial layers. *Nat. Photon.* **6**, 610–614 (2012).
206. Haq, B. et al. Micro-transfer-printed III–V-on-silicon C-band semiconductor optical amplifiers. *Laser Photon. Rev.* **14**, 1900364 (2020).
207. Baumgartner, Y. et al. High-speed CMOS-compatible III–V on Si membrane photodetectors. *Opt. Express* **29**, 509–516 (2021).
208. Goyvaerts, J. et al. Transfer-print integration of GaAs pin photodiodes onto silicon nitride waveguides for near-infrared applications. *Opt. Express* **28**, 21275–21285 (2020).
209. Yang, H. et al. Transfer-printed stacked nanomembrane lasers on silicon. *Nat. Photon.* **6**, 615–620 (2012).
210. Bae, S.-H. et al. Graphene-assisted spontaneous relaxation towards dislocation-free heteroepitaxy. *Nat. Nanotechnol.* **15**, 272–276 (2020).
211. Shin, J. et al. Vertical full-colour micro-LEDs via 2D materials-based layer transfer. *Nature* **614**, 81–87 (2023).
- This study reports a vertically stacked photonic nanomembrane system for full-colour microLEDs with ultrahigh pixel density.**
212. Yoon, J. et al. GaAs photovoltaics and optoelectronics using releasable multilayer epitaxial assemblies. *Nature* **465**, 329–333 (2010).
213. Kim, M., Seo, J.-H., Singiseti, U. & Ma, Z. Recent advances in free-standing single crystalline wide band-gap semiconductors and their applications: GaN, SiC, ZnO, β -Ga₂O₃, and diamond. *J. Mater. Chem. C* **5**, 8338–8354 (2017).
214. Liu, Q. et al. Design of micro-nano grooves incorporated into suspended GaN membrane for active integrated optics. *AIP Adv.* **8**, 115118 (2018).
215. Han, X., Fu, W., Zou, C.-L., Jiang, L. & Tang, H. X. Microwave-optical quantum frequency conversion. *Optica* **8**, 1050–1064 (2021).
216. Dong, M. et al. High-speed programmable photonic circuits in a cryogenically compatible, visible–near-infrared 200 mm CMOS architecture. *Nat. Photon.* **16**, 59–65 (2022).
217. Thompson, J. et al. Strong dispersive coupling of a high-finesse cavity to a micromechanical membrane. *Nature* **452**, 72–75 (2008).
218. Lin, Y. et al. Optimized performances in InGaN/GaN quantum-well membrane based vertical optoelectronics by the piezo-phototronic effect. *Nano Energy* **89**, 106454 (2021).
219. Ji, D. et al. Freestanding crystalline oxide perovskites down to the monolayer limit. *Nature* **570**, 87–90 (2019).
220. Srinivasan, K. & Stadler, B. J. Magneto-optical materials and designs for integrated TE- and TM-mode planar waveguide isolators: a review. *Optical Mater. Express* **8**, 3307–3318 (2018).
221. Saravi, S., Pertsch, T. & Setzpfandt, F. Lithium niobate on insulator: an emerging platform for integrated quantum photonics. *Adv. Optical Mater.* **9**, 2100789 (2021).
222. Satzinger, K. J. et al. Quantum control of surface acoustic-wave phonons. *Nature* **563**, 661–665 (2018).
223. Koechlin, M., Sulser, F., Sitar, Z., Poberaj, G. & Gunter, P. Free-standing lithium niobate microring resonators for hybrid integrated optics. *IEEE Photon. Technol. Lett.* **22**, 251–253 (2010).
224. Jia, R. et al. Van der Waals epitaxy and remote epitaxy of LiNbO₃ thin films by pulsed laser deposition. *J. Vac. Sci. Technol. A* **39**, 040405 (2021).
225. Lu, Q. et al. Engineering magnetic anisotropy and emergent multidirectional soft ferromagnetism in ultrathin freestanding LaMnO₃ films. *ACS Nano* **16**, 7580–7588 (2022).
226. Erdem, D. et al. CoFe₂O₄ and CoFe₂O₄-SiO₂ nanoparticle thin films with perpendicular magnetic anisotropy for magnetic and magneto-optical applications. *Adv. Funct. Mater.* **26**, 1954–1963 (2016).
227. Wang, Z. et al. Piezo-phototronic UV/visible photosensing with optical-fiber–nanowire hybridized structures. *Adv. Mater.* **27**, 1553–1560 (2015).
228. Zhang, Y. et al. Piezo-phototronic effect-induced dual-mode light and ultrasound emissions from ZnS:Mn/PMN–PT thin-film structures. *Adv. Mater.* **24**, 1729–1735 (2012).
229. Mak, K. F., He, K., Shan, J. & Heinz, T. F. Control of valley polarization in monolayer MoS₂ by optical helicity. *Nat. Nanotechnol.* **7**, 494–498 (2012).
230. Baugher, B. W. H., Churchill, H. O. H., Yang, Y. & Jarillo-Herrero, P. Optoelectronic devices based on electrically tunable p–n diodes in a monolayer dichalcogenide. *Nat. Nanotechnol.* **9**, 262–267 (2014).
231. Kumar, P. et al. Light–matter coupling in large-area van der Waals superlattices. *Nat. Nanotechnol.* **17**, 182–189 (2022).
232. Hwang, H. Y. et al. Emergent phenomena at oxide interfaces. *Nat. Mater.* **11**, 103–113 (2012).
233. Wen, B. et al. Ferroelectric-driven exciton and trion modulation in monolayer molybdenum and tungsten diselenides. *ACS Nano* **13**, 5335–5343 (2019).
234. Xiao, Z., Song, J., Ferry, D. K., Ducharme, S. & Hong, X. Ferroelectric-domain-patterning-controlled Schottky junction state in monolayer MoS₂. *Phys. Rev. Lett.* **118**, 236801 (2017).

235. Li, D. et al. Polar coupling enabled nonlinear optical filtering at MoS₂/ferroelectric heterointerfaces. *Nat. Commun.* **11**, 1422 (2020).
236. Ye, Y. et al. Electrical generation and control of the valley carriers in a monolayer transition metal dichalcogenide. *Nat. Nanotechnol.* **11**, 598–602 (2016).
237. Li, J.-X. et al. Electric control of valley polarization in monolayer WSe₂ using a van der Waals magnet. *Nat. Nanotechnol.* **17**, 721–728 (2022).
238. Zhao, C. et al. Enhanced valley splitting in monolayer WSe₂ due to magnetic exchange field. *Nat. Nanotechnol.* **12**, 757–762 (2017).
239. Norden, T. et al. Giant valley splitting in monolayer WS₂ by magnetic proximity effect. *Nat. Commun.* **10**, 4163 (2019).
240. Hu, G. et al. Coherent steering of nonlinear chiral valley photons with a synthetic Au–WS₂ metasurface. *Nat. Photon.* **13**, 467–472 (2019).
241. Hong, X. et al. Structuring nonlinear wavefront emitted from monolayer transition-metal dichalcogenides. *Research* <https://doi.org/10.34133/2020/9085782> (2020).
242. Chen, Y. et al. Chirality-dependent unidirectional routing of WS₂ valley photons in a nanocircuit. *Nat. Nanotechnol.* **17**, 1178–1182 (2022).
243. Basov, D. N., Fogler, M. M. & García de Abajo, F. J. Polaritons in van der Waals materials. *Science* **354**, aag1992 (2016).
244. Hu, G., Krasnok, A., Mazor, Y., Qiu, C.-W. & Alù, A. Moiré hyperbolic metasurfaces. *Nano Lett.* **20**, 3217–3224 (2020).
245. Dai, S. et al. Graphene on hexagonal boron nitride as a tunable hyperbolic metamaterial. *Nat. Nanotechnol.* **10**, 682–686 (2015).
246. Ruta, F. L. et al. Surface plasmons induce topological transition in graphene/α-MoO₃ heterostructures. *Nat. Commun.* **13**, 3719 (2022).
247. Dubrovkin, A. M., Qiang, B., Krishnamoorthy, H. N. S., Zheludev, N. I. & Wang, Q. J. Ultra-confined surface phonon polaritons in molecular layers of van der Waals dielectrics. *Nat. Commun.* **9**, 1762 (2018).
248. Zhang, Q. et al. Hybridized hyperbolic surface phonon polaritons at α-MoO₃ and polar dielectric interfaces. *Nano Lett.* **21**, 3112–3119 (2021).
249. Li, P. et al. Reversible optical switching of highly confined phonon–polaritons with an ultrathin phase-change material. *Nat. Mater.* **15**, 870–875 (2016).
250. Aghamiri, N. A. et al. Reconfigurable hyperbolic polaritonics with correlated oxide metasurfaces. *Nat. Commun.* **13**, 4511 (2022).
251. Massicotte, M. et al. Picosecond photoresponse in van der Waals heterostructures. *Nat. Nanotechnol.* **11**, 42–46 (2016).
252. Gao, A. et al. Observation of ballistic avalanche phenomena in nanoscale vertical InSe/BP heterostructures. *Nat. Nanotechnol.* **14**, 217–222 (2019).
253. Lukman, S. et al. High oscillator strength interlayer excitons in two-dimensional heterostructures for mid-infrared photodetection. *Nat. Nanotechnol.* **15**, 675–682 (2020).
254. Jiao, H. et al. HgCdTe/black phosphorus van der Waals heterojunction for high-performance polarization-sensitive midwave infrared photodetector. *Sci. Adv.* **8**, eabn1811 (2022).
255. Sarker, B. K. et al. Position-dependent and millimetre-range photodetection in phototransistors with micrometre-scale graphene on SiC. *Nat. Nanotechnol.* **12**, 668–674 (2017).
256. Jiang, H. et al. Enhanced photogating effect in graphene photodetectors via potential fluctuation engineering. *ACS Nano* **16**, 4458–4466 (2022).
257. Jiang, Y. et al. Coexistence of photoelectric conversion and storage in van der Waals heterojunctions. *Phys. Rev. Lett.* **127**, 217401 (2021).
258. Wei, J. et al. Zero-bias mid-infrared graphene photodetectors with bulk photoresponse and calibration-free polarization detection. *Nat. Commun.* **11**, 6404 (2020).
259. Wei, J. et al. Geometric filterless photodetectors for mid-infrared spin light. *Nat. Photon.* **17**, 171–178 (2023).
- This study reports geometric filterless photodetectors for circularly polarized light; a specific circularly polarized light response was realized using a plasmonic nanostructure array with designed symmetry.**
260. Wang, S. et al. Two-dimensional devices and integration towards the silicon lines. *Nat. Mater.* **21**, 1225–1239 (2022).
261. Xiong, L. et al. Programmable Bloch polaritons in graphene. *Sci. Adv.* **7**, eabe8087 (2021).
262. Song, J. et al. Efficient excitation of multiple plasmonic modes on three-dimensional graphene: an unexplored dimension. *ACS Photon.* **3**, 1986–1992 (2016).
263. Wetzstein, G. et al. Inference in artificial intelligence with deep optics and photonics. *Nature* **588**, 39–47 (2020).
264. Jiang, J. et al. Carrier lifetime enhancement in halide perovskite via remote epitaxy. *Nat. Commun.* **10**, 4145 (2019).
265. Shu, H. et al. Microcomb-driven silicon photonic systems. *Nature* **605**, 457–463 (2022).

Acknowledgements

S.-H.B. thanks the Institute of Materials Science and Engineering (IMSE), Washington University in St Louis, for support. C.-W.Q. acknowledges support from the National Research Foundation Singapore (CRP26-2021-0004). D.-H.K. thanks support from Korea Institute for Advancement of Technology (KIAT) grant funded by the Korea Government (MOTIE) (PO017305, Human Resource Development Program for Industrial Innovation (Global)).

Author contributions

Y.M., J.F., S.H., Z.X., T.Z., W.M., Y.Z., J.S.K., I.R., D.-H.K., C.-W.Q. and S.-H.B. researched data for the article. Y.M., J.F., S.-H.B., C.-W.Q. and L.Y. contributed substantially to discussion of the content. Y.M., J.F., S.-H.B., C.-W.Q., L.Y., J.-W.L., S.H., Z.X. and W.M. wrote the article. Y.M., S.-H.B., C.-W.Q., L.Y., J.-W.L. and Y.Y. reviewed and edited the manuscript before submission.

Competing interests

The authors declare no competing interests.

Additional information

Supplementary information The online version contains supplementary material available at <https://doi.org/10.1038/s41578-023-00558-w>.

Peer review information *Nature Reviews Materials* thanks the anonymous reviewers for their contribution to the peer review of this work.

Publisher's note Springer Nature remains neutral with regard to jurisdictional claims in published maps and institutional affiliations.

Springer Nature or its licensor (e.g. a society or other partner) holds exclusive rights to this article under a publishing agreement with the author(s) or other rightsholder(s); author self-archiving of the accepted manuscript version of this article is solely governed by the terms of such publishing agreement and applicable law.

© Springer Nature Limited 2023

¹Mechanical Engineering and Materials Science, Washington University in St Louis, St Louis, MO, USA. ²Department of Electrical and Computer Engineering, National University of Singapore, Kent Ridge, Singapore. ³Institute of Materials Science and Engineering, Washington University in St Louis, St Louis, MO, USA. ⁴Department of Electrical and Systems Engineering, Washington University, St Louis, MO, USA. ⁵Department of Materials Science and Engineering and California Nano Systems Institute, University of California Los Angeles, Los Angeles, CA, USA. ⁶School of Chemical Engineering, Sungkyunkwan University, Suwon, South Korea. ⁷Biomedical Institute for Convergence, Sungkyunkwan University, Suwon, Republic of Korea. ⁸Department of Nano Science and Technology and Department of Nanoengineering, SKKU Advanced Institute of Nanotechnology (SAINT), Sungkyunkwan University, Suwon, Republic of Korea. ⁹SKKU Institute of Energy Science & Technology (SIEST), Sungkyunkwan University, Suwon, Republic of Korea. ¹⁰These authors contributed equally: Yuan Meng, Jiangang Feng, Sangmoon Han.